Hardware Design and Implementation of an Electromagnetic Levitation System in an Additive Manufacturing Environment

by

Saksham Malik

A thesis
presented to the University of Waterloo
in fulfillment of the
thesis requirement for the degree of
Masters of Applied Science
in
Mechanical Engineering

Waterloo, Ontario, Canada, 2022

Author's Declaration

I hereby declare that I am the sole author of this thesis. This is a true copy of the thesis, including any required final revisions, as accepted by my examiners.

I understand that my thesis may be made electronically available to the public.

Abstract

Magnetic Levitation and Additive Manufacturing are two promising fields with ever growing interest in several industrial settings. There is, however, negligible overlap between the two fields. This research aims to combine the ability of electromagnetism to successfully levitate an aluminum disc using Electrodynamic Suspension (EDS), with Laser Powder Bed Fusion (LPBF) based additive manufacturing to enhance the complexity of fabricated objects. This provides a higher degree of freedom for manufacturing, and gives the user the ability to deposit material on the flip side of substrate, all through just one print activity.

Electromagnetic system designed for this research comprises of two sets of oppositely wound concentric coils, seated in a pure-iron core. An aluminum disc is selected for levitation purposes due to its high compatibility with the additive manufacturing environment. ANSYS Maxwell, a FEMM based software is selected for design of the system. The coils are optimized for high levitation forces in the axial (Z-axis) direction, as well as restoration forces in the lateral (R-axis) direction using a $5A_{RMS}$ input supply, in the range of 50 - 1000Hz. A thermal analysis is conducted to ensure system suitability for 20 minutes of activity in an additive manufacturing machine.

Intrinsic coil parameters such as inductance and its reactance effects are investigated through resonant frequency and time constant step response analyses. Low and high voltage experiments are conducted to correlate system output current and magnetic field density with simulations. An enclosure is constructed according to CSA (Canadian Standards Association) guidelines to perform experiments at $300V_{RMS}$, 1.5kW.

Experimental debugging is performed to tune system performance to optimal capability.

The relative permeability of the core is studied at low magnetic field density outputs and corrected accordingly. The strength of coils is established, and magnetomotive force of the overall system is increased using a custom variable resistor setup in parallel with one set of coils. The levitative ability of the system is improved and matched to simulations. Finally, levitation is accomplished, with and without a payload suspension, to show viability for additive manufacturing applications.

Future work is discussed to expand further on current progress and highlight drawbacks of the established system. Recommendations are made to modify system components based on their material and geometric characteristics. A possible control model is discussed to ensure stability of levitation. The viability of magnetic levitation for additive manufacturing is hence established, and novel results are presented.

Acknowledgements

I would like to take this opportunity to thank each and every person I got a chance to work with, to help me earn my Master's degree. A big thank you, and all my respects for Dr. Behrad Khamesee and Dr. Ehsan Toyserkani, whose constant support and guidance were the main reasons I have come so far. A special acknowledgement goes out for Ph. D. candidate, and my colleague Parichit Kumar, who was extremely helpful and dedicated in every step of the way.

I would also like to thank Electronics Technician and research staff member Neil Griffett, as well as Rob from MCI Ltd., who were very resourceful throughout this research.

Last but not the least, I would like to thank all my lab members - Parichit, Azeem, Pooriya, Heba, Daniel, Chanuphon, Curtis, Bob, Moslem and Yashesh; it was a pleasure working with each and every one of them.

This work is funded by Holistic Innovation for Additive Manufacturing (HI-AM) through Natural Sciences and Engineering Research Council of Canada (NSERC) and Canada Foundation for Innovation (CFI).

Dedication

This thesis is dedicated to my parents, my sister and my dear friends, who have guided me through my journey of earning my Master's degree. This would not be possible without their love and support.

This is also specially dedicated to my grandmother, whose love and blessings will stay with me forever.

Contents

Author's Declaration ii

Abstract iii

Acknowledgements v

Dedication vi

List of Figures x

List of Tables xv

1 Introduction 1

1.1 Introduction to Magnetic Levitation 1

1.1.1 Diamagnetic materials 2

1.1.2 Ferromagnetic materials 2

1.1.3 Paramagnetic materials 3

1.2 Types of Levitation 4

1.2.1 Electro Magnetic Suspension 4

1.2.2 Electro Dynamic Suspension 4

1.3 Additive Manufacturing 5

1.4 Contribution of this Thesis 6
1.5 Objective and Thesis Outline 9

2 Theory and Literature Review **14**
2.1 Relevant Scientific Laws 14
2.1.1 Ampere's Circuital Law 15
2.1.2 Faraday's Law 16
2.1.3 Lenz's Law 17
2.1.4 The Principle of Lorentz Force 17
2.2 Earnshaw's Theorem 18
2.3 Magnetic Levitation of different geometries 18
2.3.1 Levitation of a coil 19
2.3.2 Levitation of a sphere 20
2.3.3 Levitation of a disc 21

3 System Design **24**
3.1 Selection of ANSYS Maxwell as a reliable software 25
3.2 Setup Design 27
3.2.1 Coil Design 31
3.2.2 Core selection 40
3.2.3 Disc Design 42

4 Thermal Analysis **45**
4.1 Necessity for Thermal Analysis 45
4.1.1 Coil DC Resistance 45
4.1.2 Effect of Temperature on Core Permeability 47
4.1.3 Epoxy Protection 48

4.2 System Thermals . . . 48
4.2.1 Coil Thermals . . . 49
4.2.2 Core Thermals . . . 50
4.3 Net System Loss . . . 52
4.4 Disc Thermals . . . 54

5 Experimental Setup **57**
5.1 Hardware Selection . . . 58
5.1.1 Power Supply Selection . . . 59
5.1.2 Gaussmeter selection . . . 60
5.1.3 Oscilloscope and Current Sensor . . . 60
5.2 Low-Voltage Experiments . . . 61
5.3 High-Voltage Experiments . . . 62
5.4 Inductance Measurement . . . 63
5.4.1 Series resonant frequency . . . 66
5.4.2 Time Constant Experiment . . . 68
5.4.3 ANSYS Maxwell Matrix Inductance . . . 69
5.5 Enclosure construction for AM environment compatibility . . . 70

6 Electrical Calibration **73**
6.1 Levitation Attempts at 50Hz and 1000Hz . . . 73
6.1.1 Levitation at 50Hz . . . 74
6.1.2 Levitation at 1000Hz . . . 74
6.2 Magnetic Permeability Calibration . . . 75
6.3 Strength of Coils – Magnetomotive Force . . . 79
6.3.1 Trade-off between levitation and restoration – analytical model . . . 79

6.3.2 Variable Resistor Enclosure 83
6.4 Successful Levitation 84
6.5 Levitation with Payload 86

7 Conclusions and Future Work **90**
7.1 Summary 90
7.2 Discussion 91
7.3 Future Work 92

References **99**

Appendices **100**

A Coil and Core Schematics **101**

List of Figures

1.1 A patent presented by The Boeing Company introducing the validity of using magnetic levitation for additive manufacturing applications [8]. The numbers mentioned in the image correspond to various labels mentioned in the patent. These labels discuss the substrate, the levitation system, the electrical and mechanical subsystems, and so on 7

1.2 Intended electromagnetic levitation for additive manufacturing 9

1.3 Work-flow for this research 12

2.1 Ampere's Law 16

2.2 A 2D axis-symmetric representation of the Marc T. Thompson system [11] 19

2.3 A visual representation of the Witteveen research cited in [16] 20

2.4 A planar section of the system with anti-parallel coils, embedded in an iron core [18] 21

2.5 TOP VIEW - Intended system for design 23

3.1 Manufacutred electromagnetic coils 25

3.2 ANSYS Maxwell validation of Marc T. Thompson's reference paper [11] . . 26

3.3 ANSYS Maxwell validation of Ghayoor's reference paper [17] 27

3.4 Magnetic field at a point on axis of a circular current carrying coil 29

3.5 Figure a) shows superposition of magnetic fields at a point 'A' imagined along the axis of the coils. Figure b) shows superposition of magnetic fields at a point 'B' imagined off-axis, closer to the secondary coil. 30

3.6 Skin depth effect [19] . . . 32
3.7 G - Factor as a contour function of the geometric properties of the system presented in [20] . . . 33
3.8 Figure a) shows inner coil width optimization and figure b) shows outer coil width optimization vs levitation force . . . 35
3.9 Inner and outer coil radial placement shown as a ratio of R2/R1 vs levitation force . . . 36
3.10 Base Core Optimization . . . 37
3.11 2-D axis-symmetric view of the coils in ANSYS Maxwell . . . 38
3.12 Levitation Force comparison between cases 1 and 2 presented in 3.2.1 . . . 40
3.13 Comparison of different materials . . . 42
3.14 Disc Levitation forces as a function of radii and heights, at various frequencies 44

4.1 Variation of Resistance and Current with Temperature . . . 46
4.2 Variation of permeability of iron with temperature [23] . . . 47
4.3 Circuit Diagram . . . 49
4.4 Figure a) shows the net power loss from a resistive element in a purely resisitve circuit, whereas figure b) the net power loss and return from an indcuctive element in a purely inductive circuit . . . 50
4.5 Phasor diagram and, voltage and current waveforms with phase shift for these electromagnetic coils. Phasor diagram not to scale . . . 51
4.6 Temperature contour of system after 20 minutes of operation . . . 53
4.7 Temperature variation of system over 20 minutes of operation . . . 54
4.8 Current Density plot of a 2D axis-symmetric cross-section of half the disc . 55
4.9 Temperature contour of the disc after 20 minutes . . . 55
4.10 Temperature variation of disc over 20 minutes of operation . . . 56

5.1 Experimental setup schematic . . . 58

5.2 BK Precision 9832B Power Supply 59
5.3 Current vs Voltage, Magnetic Field Density comparison at 50Hz and 1000Hz: Experiments and Simulations 62
5.4 Current vs Voltage, Magnetic Field Density comparison at 50Hz: Experiments and Simulations 63
5.5 Long multiple-layer coil 65
5.6 At 420Hz, the inductive and capacitive reactances negate each other's effects. Hence, Z = R, and L = 0.1436H 66
5.7 At 420Hz, the votlage and current waveforms overlap each other with a $20\mu s$ (or 3.024°) shift 68
5.8 Step response of the current 69
5.9 Coils on top of the built enclosure 71
5.10 Deformation response of the enclosure under the weight of the coils 72

6.1 ANSYS Maxwell using iron core with a relative permeability of 9400 76
6.2 The B-H curve of the pure iron core as obtained from the supplier. The green portion of the curve is where this system functions, the blue portion of the curve is the ideal linear region 77
6.3 Indication of no levitation at 300V RMS, 50Hz with the current strength of coils 80
6.4 Self-restoration of disc upon application of a manual external force displacing it from its origin 81
6.5 Depiction of Tradeoff between Levitation and Restoration behavior of the system. Not to scale. 82
6.6 Circuit model of the coils with a 40Ω resistor in parallel to the outer coil . 83
6.7 ANSYS Maxwell simulations at 300V RMS, 85Hz 85
6.8 Successful experimental levitation of disc observed at 300V RMS, 85Hz . . 86
6.9 ANSYS Maxwell simulations with added **15.2g payload**, at 300V RMS, 85Hz 87

6.10 Successful experimental levitation of disc with **15.2g** added payload observed at 300V RMS, 85Hz 88

6.11 Successful simulation of levitation of disc with **5g**, **10g**, **25g**, and **50g** added payload observed at 300V RMS, 85Hz 89

7.1 Possible control system using sensor feedback for future iterations of coils . 94

List of Tables

3.1 Table of constraints 28

3.2 Parametrization of Coil Dimensions 34

3.3 Finalized Coil Dimensions 39

4.1 Power Ferrite Core loss model properties 52

5.1 Inductance 70

6.1 Magnetic Field Density at the tip of coils: Experiments vs Simulations . . 75

6.2 Magnetic Field Density at the tip of coils at 300V, 50Hz: Simulations with different core permeabilities. Error percentages are in comparison with experimental observations 78

6.3 Magnetic Field Density at the tip of coils: Simulations with different input voltages. Error percentages are in comparison with experimental observations 79

Chapter 1

Introduction

1.1 Introduction to Magnetic Levitation

Magnetic levitation is a process by which an object is suspended mid-air by using magnetic fields. It occurs when the magnetic fields from a permanent magnet, or a magnetized substance, are aligned in a direction, such that it counteracts the effects of gravitational force on the levitated object.

This technique has found a number of applications in today's world. It is used in several industries such as transportation, robotics, biomedical engineering, etc. The purpose of using magnets is to eliminate contact between two surfaces, hence, getting rid of losses due to friction. This leads to more energy efficient design solutions.

There are a few ways this can be accomplished successfully. These methods differ on the basis of the type of material subjected to levitation. Different materials may have different

relative magnetic permeability μ_r, which affects the manner in which they can be levitated.

1.1.1 Diamagnetic materials

Diamagnetic materials have a relative magnetic permeability μ_r <1. These materials are generally non-magnetic in nature, such as water, diamond, and plastic. Diamagnetic materials tend to be repelled by any external magnetic fields as mentioned in [1]. They tend to be attracted towards the field minima. However, these materials can accomplish levitation by directly counteracting the Earnshaw's theorem which stands true for paramagnetic materials. Paramagnetic materials tend to be attracted towards the field maxima of a magnetic source, but since this maxima occurs only at the field sources, this levitation is not stable as mentioned in [1]. On the other hand, the induced magnetic moments inside a diamagnetic substance are aligned in a direction opposite to the external magnetic field, and hence, create a force of repulsion. If this force is strong enough, the diamagnetic material can be levitated stably against the gravitational force.

1.1.2 Ferromagnetic materials

Ferromagnetic materials have a very high relative magnetic permeability μ_r >>1 ($\approx 100 - 10000$). These are most ferrous metals such as iron, cobalt, nickel and some alloys, such as steel. The electrons in a ferromagnetic material become aligned in the direction of an applied external magnetic field. In other words, the internally induced dipoles are in compliance with the external field, hence, establishing a denser magnetic field, especially at the surface. A permanent magnet is also a ferromagnetic substance, which has

permanently aligned magnetic dipoles, hence, creating a permanent field. Over the years, ferromagnetic substances have found a number of uses in domestic, commercial as well as industrial environments. Motors work on the principle of using a rotational motion caused by induction of magnetic fields using ferromagnetic cores. Electric generators, transformers, telephones, etc. too use ferromagnetic materials for major functions.

1.1.3 Paramagnetic materials

Paramagnetic materials have a relative magnetic permeability $\mu_r > 1$. These materials are generally metallic in nature, such as aluminum, magnesium, lithium etc. These kind of materials are very faintly attracted towards a magnetic field, and seldom act as temporary magnets. But being electrically conductive in nature, this property can be used in conjunction with Faraday's law. According to [2], a paramagnetic substance introduced to a magnetic field will oppose the change to its current state of zero currents flowing through it. This causes a generation of an electromotive force which produces a magnetic field in a direction opposite to the external magnetic field. This phenomenon depends directly on the rate of change of magnetic field through the object. Using this technique, an object can potentially be levitated if a stable magnetic field is created.

This research uses an alternating current based system with two coils wound in opposite directions, to generate time-varying magnetic fields. This causes eddy currents to flow through the volume of a paramagnetic Aluminum disc, causing it to levitate. This is discussed further in section 1.2, as electrodynamic suspension is used to levitate the disc.

1.2 Types of Levitation

There are two main types of magnetic levitation technology in use today - Electro Magnetic Suspension and Electro Dynamic Suspension. They differ in the manner they occur, the functions they can perform, as well as the materials they can be used with.

1.2.1 Electro Magnetic Suspension

This is a technique by which an objected is suspended mid-air using an external attractive force [3]. Usually the object subjected to this method of levitation is ferromagnetic in nature, due to which, this cannot be used for objects made of other materials, such as Aluminum, which will be discussed in great detail in this thesis.

1.2.2 Electro Dynamic Suspension

In this technique, an object is levitated using an external repulsive force [4]. This technique is more feasible as it enables the levitation of materials which are not just ferromagnetic. For objects that do not have an intrinsic magnetism, eddy-currents can be generated throughout their volume, which create their own magnetic field in opposition to the external magnetic field, enabling repulsion. This method has garnered more attention in the world of magnetic levitation based transportation, as it provides an unstable levitation, which can be used for propulsion. Electro dynamic suspension is also of primary significance to this research as it can be used in conjunction with additive manufacturing compatible materials such as Aluminum.

1.3 Additive Manufacturing

Additive Manufacturing is a process used to create 3-dimensional geometries with micro-metric precision. It is garnering a lot interest in every major field of science, as it can be used to produce extremely complex geometries, which are otherwise difficult, or impossible to produce through one or more traditional manufacturing processes. The main advantage possessed by this technique is the fact that it can produce 3-D models of any imaginable object through a single print process. On the other hand, the same object developed through traditional methods of manufacturing may require extensive post processing, such as subtractive manufacturing. AM still has some disadvantages compared to traditional manufacturing processes, such as cost of manufacturing, complications with printing overhanging geometries, strength of parts, etc.

Additive Manufacturing has evolved from being used primarily for prototype generation, to more viable options for industrial, commercial or medical applications. This technique is being utilized for developing bio-compatible Titanium alloys as bone replacements for people with amputations, as strong yet light bone structures can be manufactured through AM practices [5]. It can also be used to make airplane turbines in one go, without the need for assembly of multiple smaller parts[6]. AM is also being used to print concrete in the construction business [7].

Despite its presence in multiple fields, additive manufacturing has had negligible overlap with the field of electromagnetism. These are two significant fields in the world of science, and can be combined to create optimized solutions for metal-based manufacturing.

1.4 Contribution of this Thesis

As mentioned earlier, the application of magnetic levitation in the field of manufacturing has found little to no use. Additionally, additive manufacturing being an up and coming field, requires enhancements to make its benefits exceed the disadvantages of employing its technique over traditional manufacturing processes. Combining the positional maneuverability of a suspended body using magnetic levitation with the high-level manufacturing manipulation achieved through additive manufacturing is a compelling prospect.

A patent filed by Boeing referenced at [8] indicates the validity of such a system. This patent mentions the possibility of levitating an object through electromagnetic levitation while using additive manufacturing techniques to create an entire part, or a feature of a part by printing material into space. This is achieved by suspending the part mid-air using acoustic and electromagnetic levitation methods, the latter of which is the focus of this thesis. These steps are repeated all the while changing the spatial orientation of the part due to the added degree of freedom in the axial as well as rotational directions, as shown in figure 1.1. Along with an increase in maneuverability, the part also requires minimal to no post-processing actions since the substrate is printed into the part as its inner component. Hence, no print-bed is required either, which saves on time for maintenance and cleaning before printing multiple parts. Despite being a promising avenue, this idea has not been realized in any research project so far. The research mentioned in this thesis aims to realize the viability of this project, by creating such an electromagnetic levitation system for stable levitation of a disc, for applications in additive manufacturing environments.

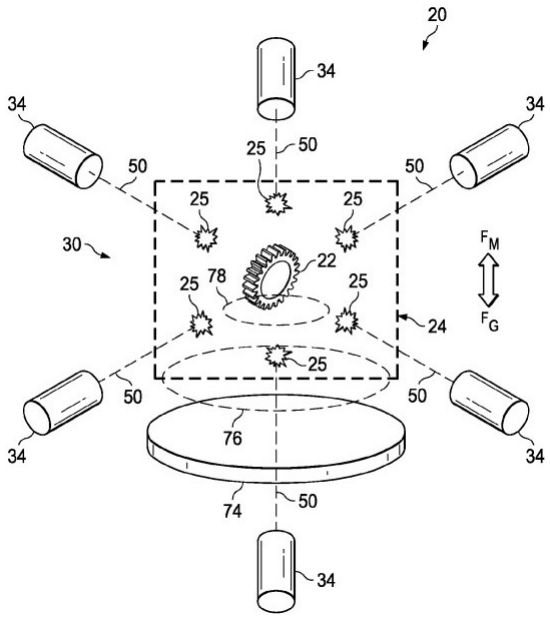

Figure 1.1: A patent presented by The Boeing Company introducing the validity of using magnetic levitation for additive manufacturing applications [8]. The numbers mentioned in the image correspond to various labels mentioned in the patent. These labels discuss the substrate, the levitation system, the electrical and mechanical subsystems, and so on

This research contributes to the fields of electromagnetic levitation and additive manufacturing by combining the respective critical aspects and creating a novel technique. The first contribution of this thesis is to invert and integrate the postulates of Earnshaw's theorem into creating a self-sustaining magnetic levitation system. This is necessary to create the required foundation for the research.

Secondly, this thesis presents a method of using fixed variable parametrization in order to create an optimized coil setup in order to facilitate the required levitation. This is necessary since the coil levitator system will be used inside an additive manufacturing machine which has a limited base area for setup.

Thirdly, the manufactured coils will be tested at low voltages, including a self-resonance check to study the intrinsic properties of the coil. And finally, results from the selected FEM software for electromagnetic simulation analyses will be compared with results from experimental analyses conducted on the manufactured coils. This is important to ensure that the coil functions in the desired manner. The coils are intended to function in a manner to produce time-varying magnetic fields, which induce eddy currents through the volume of the disc. The disc in turn, produces its own time-varying magnetic fields which counter the parent magnetic field, and thus levitates.

It must be noted that magnetic levitation and additive manufacturing (AM) are two very promising fields of science and engineering, with minimal overlap. This research aims to bridge the gap between the two by utilizing the maneuverability offered through the use of magnetic levitation for additive manufacturing. The substrate, which is fixed in a metal-based Directed Energy Deposition type of AM, is levitated through magnetic

levitation, and thus provided with an added degree of freedom in the axial and rotational directions. It is important to note that the degree of freedom presented in this research is restricted to just one level - axial, which can be done by controlling current to manipulate the substrate's axial position. This is the case as this research aims to provide only the initial groundbreaking to bridge the two fields. In future iterations of this research, it would be possible to levitate and manipulate the spatial orientation of the substrate with additional 6 degrees of freedom.

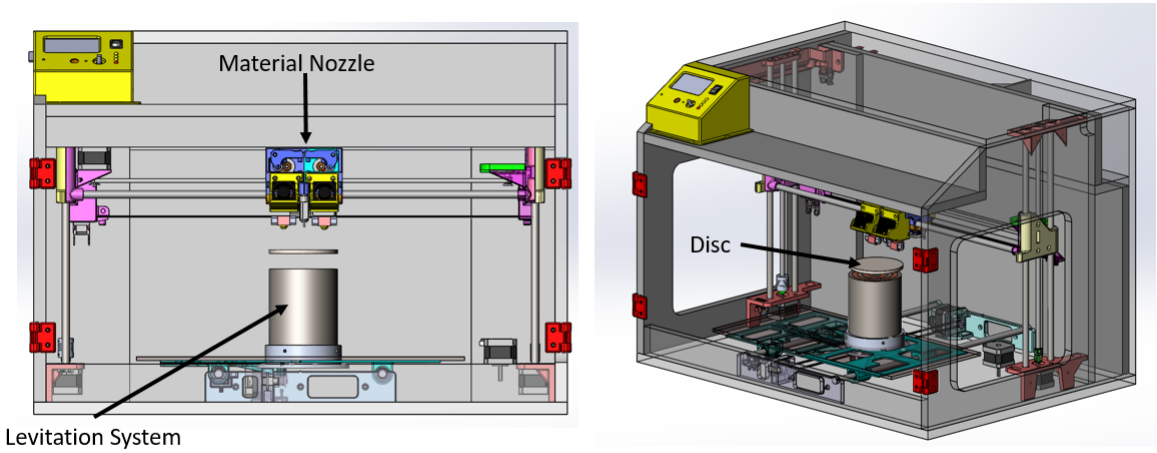

A. Front View: MagLev System in AM enclosure

B. Isometric View: MagLev System in AM enclosure

Figure 1.2: Intended electromagnetic levitation for additive manufacturing

1.5 Objective and Thesis Outline

The main objective of this thesis is to prove viability of using electromagnetic levitation of a metallic substrate for use in an AM environment. As a part of this research, a small

cylindrical disc is selected as the subject for electromagnetic levitation. It is also meant to be used as a substrate for additive manufacturing, where, the disc itself becomes a part of the fabricated object.

As seen in figure 1.2, the entire electromagnetic setup is installed inside a metal additive manufacturing machine. As the image indicates, the disc is supposed to stably levitate above the coils to create a stationary base for fabrication. The 3D printing capabilities of a metal deposition machine are utilized. The [9] Direct Metal Deposition (DMD) technology developed by *DM3D* is selected for our application. This technology is a patented closed-loop feedback mechanism based system that has a high degree of resolution in fabrication of metal 3D printed objects. These objects range over a variety of industrial applications such as airplane turbines, vehicle engine blocks, aerospace rocket booster body shells, etc. The machine is currently situated at the 'Multi-Scale Additive Manufacturing' lab (or, MSAM lab) at the University of Waterloo.

The following objectives were set up as part of accomplishing the work in this research:

- Combining relevant laws, background information and reference theory to establish evidence for a magnetic levitation system
- Designing a system for magnetic levitation of a paramagnetic material using electrodynamic suspension
- Analyzing and modifying magnetomotive strength of the electromagnetic coils
- Conducting FEM analysis to compare experimental and simulation performance of disc levitation and restoration

- Implementing the designed and procured hardware for validation of system, to be used in an additive manufacturing environment

To accomplish the goal of this research, there are two main design objectives that need to be targeted:

- The disc needs to be stably levitated with in the axial direction with a maximum tolerance of $\pm 0.5mm$. Hence, the system needs to generate a significant and consistent levitation force
- The disc needs to be stably levitated in the lateral direction with minimal disturbances. Hence, the system needs to generate significant restoration forces

As indicated in figure 1.3, the system development begins with the parametrization of geometric variables in the levitator coil. This includes varying the individual coil widths, placements with respect to the central axis, and finally the height of the coils to have a stable levitation system. This is followed by impedance correction as the system comprises of a dense setup which may lead to unwanted inductive and parasitic capacitance reactance issues which impedes the current flow through the coils. Following is a flowchart depicting the work-flow of this research:

Following is a summarized description of the contents found in each chapter of this thesis:

- Chapter 1: Introduction to this research, magnetic levitation and additive manufacturing, motivation and contributions of this research

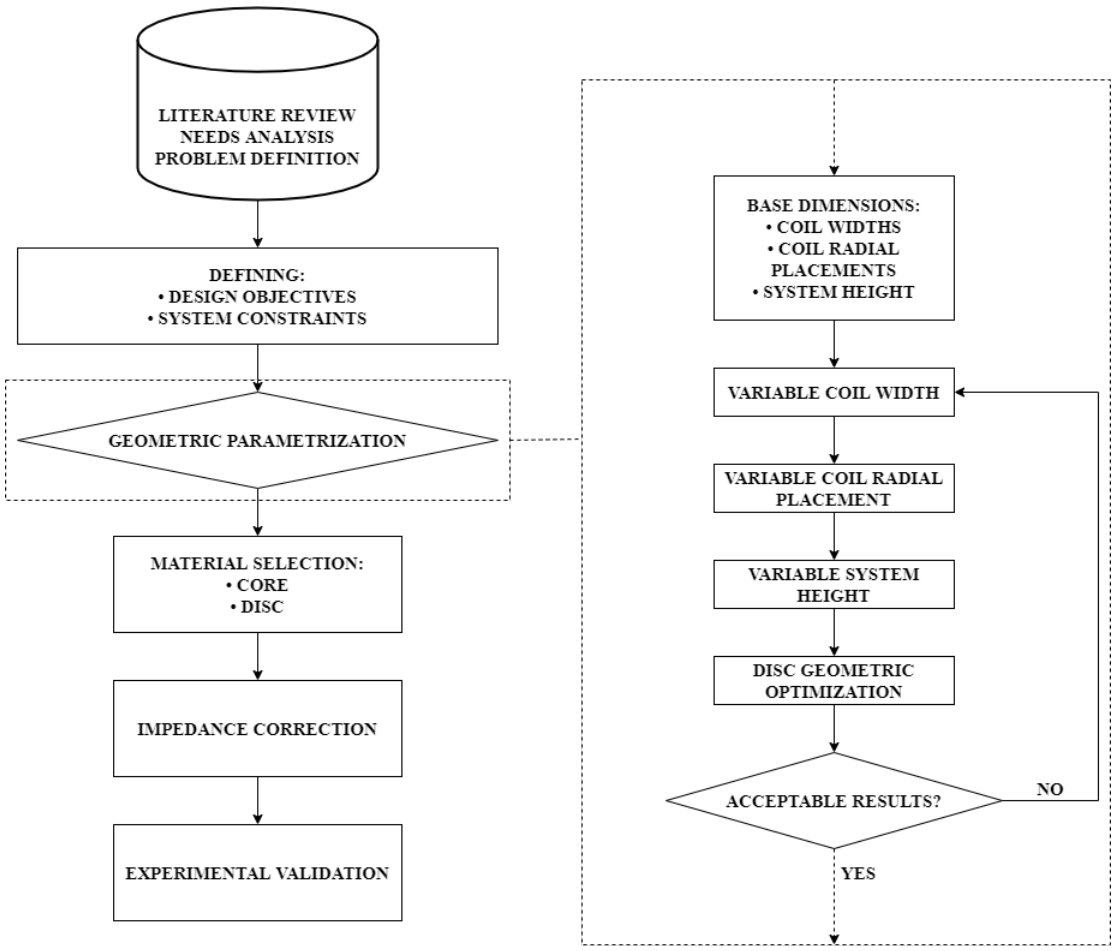

Figure 1.3: Work-flow for this research

- Chapter 2: Background and literature review, relevant laws governing electromagnetic levitation
- Chapter 3: System design, coil geometry, core material selection, optimization of disc size
- Chapter 4: Thermal Analysis of the system - coils and disc

- Chapter 5: Experimental setup, coil characteristics analysis, inductance measurement through resonant frequency and time constant step response analyses, enclosure construction
- Chapter 6: Experimental validation, calibration to adjust force of levitation and restoration, levitation of disc at 85Hz, levitation with payload suspension
- Chapter 7: Conclusions and Future Work Recommendation

Chapter 2

Theory and Literature Review

This chapter will present the relevant laws and the required background information to describe the setup of the electromagnetic levitation system. The methods used for developing the coil geometry and the relevant literature review will also be discussed, followed by a description of the design objectives and constraints, as a functional requirement for the additive manufacturing machine. Finally, the core and disc optimization will be discussed as it is relevant to the levitative force generation, and the thermal management in the system.

2.1 Relevant Scientific Laws

This research relies on four major scientific laws that have established the basis of electromagnetics.

2.1.1 Ampere's Circuital Law

Every current carrying electric wire produces a magnetic field. The prediction of the magnitude of this magnetic field was made by André-Marie Ampère, who is considered as the founder of electromagnetism. According to Ampere's Circuital Law, the line integral of magnetic field in a closed loop is equivalent to the total current passing through this loop. Mathematically,

$$\oint \vec{\mathrm{B}}\, d\vec{\mathrm{l}} = \mu_o I \tag{2.1}$$

where, $\vec{B}$ is the magnetic flux density, $d\vec{\mathrm{l}}$ is an infinitesimally small length of wire carrying current I, and μ_o is the permeability of free space. The closed loop integral of a straight current carrying wire, as shown in figure 2.1, would result in a circular path, and hence $l = 2\pi r$, where r is the shortest distance between the wire and the point where the magnetic field is being measured.

This was further explained through Maxwell's right hand Corkscrew rule, as referenced in [10], that if a fist is closed with the thumb pointing out, and the direction of current is assumed to be in the direction of the thumb, the direction of magnetic field is followed by the direction of the enclosing fingers. This relates to the system mentioned in this research, as an electric current is passed through coils to generate a magnetic field.

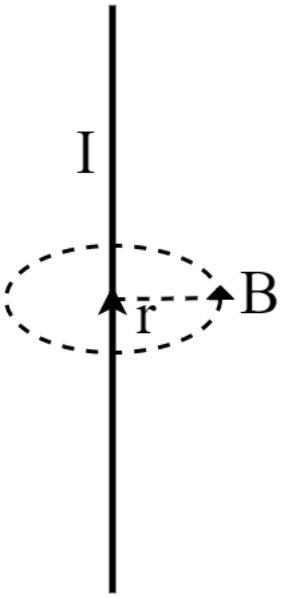

Figure 2.1: Ampere's Law

2.1.2 Faraday's Law

According to Faraday's Law, when a conductor is introduced in a region of a time-varying magnetic field, a current is induced in it in a closed loop [11]. Alternatively, when a magnetic field is varied with respect to time, a current is induced in a closed loop path in a conductor inside its region of influence. This can be visualized through Maxwell's equation as follows:

$$\nabla \times E = \nabla \times \frac{J}{\sigma} = -\frac{\delta B}{\delta t} \tag{2.2}$$

where, E is the induced electric potential, J is the induced current density, and σ is the electrical conductivity of the material passed through the influence of the time varying magnetic fields. This is relevant for the system presented in this thesis, as an alternating

current is used to generate time-varying magnetic field at an axial distance above the coils. A conducting paramagnetic Aluminum disc is used, and based on Faraday's Law, currents are induced through the volume of the disc, which in turn produce their own magnetic field.

2.1.3 Lenz's Law

Lenz's law works in conjunction with Faraday's Law. It takes the law further and predicts that the induced electric potential in the material, acts in a manner to oppose the change of magnetic fields passing through it [12]. If the magnetic field introduced through the closed loop material is increasing, the electric potential (or current) rising through the material would flow in a direction to oppose the input magnetic field, and hence, mathematically,

$$\varepsilon = -\frac{\delta \phi_B}{\delta t} \tag{2.3}$$

where, ε is the induced electromotive force, and ϕ_B is the time varying magnetic flux. Lenz's law ensures, that the magnetic field produced by the induced currents in the disc are in a direction opposite to the parent magnetic field produced by the coils.

2.1.4 The Principle of Lorentz Force

Finally, the interaction of the input and induced magnetic field as described in the earlier sections, is explained through the principle of lorentz force. According to this principle, the input and induced magnetic fields oppose each other, hence, generating a force, as referenced in [13] The principle of lorentz force is responsible for the success in many

industrial applications. The squirrel cage motor is the biggest example of a widely used electric component used in many compressors, fans, drives for low power applications, etc. Based on this principle, the two magnetic fields (produced by the coils and the disc respectively) with like poles facing each other, repel and cause disc levitation.

2.2 Earnshaw's Theorem

According to Earnshaw's theorem [14], no object can be stably levitated through the use of static magnetic fields. It is possible to get around this problem by using diamagnetic materials, or superconductors, as mentioned in [15]. It is also possible to use an external feedback system to manipulate the static fields and achieve stable suspension.

This research aims to use a set of two anti-parallel concentric current carrying coils with an AC input supply to generate time-varying magnetic fields to achieve eddy current levitation.

2.3 Magnetic Levitation of different geometries

The electromagnetic levitation of a paramagnetic substance, as mentioned in this research, is reliant on the principle of electrodynamic suspension. As explained in earlier sections, electro-dynamic suspension is garnering a lot of interest in the pursuit of creating systems to stably levitate objects. Following sections discuss the development of levitation systems for different geometries.

2.3.1 Levitation of a coil

Marc T. Thompson discusses a system to levitate a current carrying electromagnetic coil in [11]. A single loop of coil with a 26A RMS alternating current passing through it is levitated over a thick Aluminum base. This can be seen in figure 2.2. This research indicates the viability of achieving eddy-current EDS levitation. The major drawback of this system is the use of copper in the levitating object, as the object is heavier and provides a greater opposing force of gravity. Another drawback is the use of just a single coil as it cannot provide a repulsive force in the lateral direction, and any disturbance in this direction would lead to an unstable mobile system. It has good applications in setting up technology for a levitating platform to carry goods from one place to another over a flat surface.

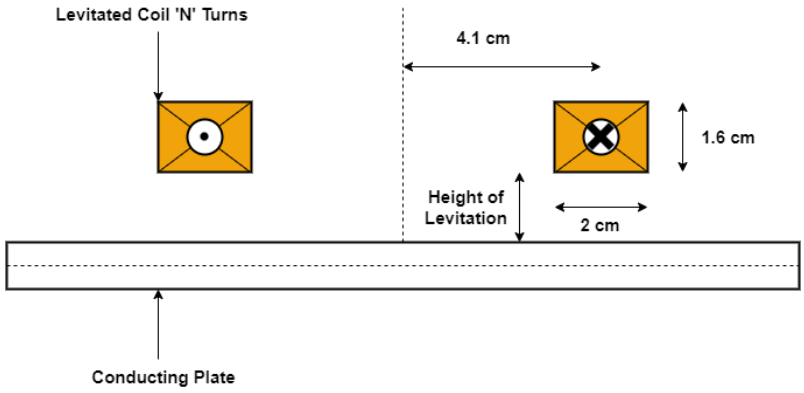

Figure 2.2: A 2D axis-symmetric representation of the Marc T. Thompson system [11]

2.3.2 Levitation of a sphere

J. P. Witteveen discusses a system to levitate a metallic sphere within the bounds of current carrying coils looped around it, as mentioned in [16]. A minimal system of coils wound in 6 turns carrying currents up to 800A RMS is created to freely suspend an Iridium sphere of 6mm. This research solves the drawback of the Marc T. Thompson research in a way that the sphere is axially and laterally suspended stably within the coils, as seen in figure 2.3. It works on the principle that eddy currents induced in the volume of the sphere are broken down into multiple smaller current loops, which produce tiny magnetic dipoles opposing the direction of input magnetic field. Despite its success, it introduces its own downsides, as the amount of current used to suspend a sphere of just 6mm is enormous. Moreover, this system would interfere with the additive manufacturing application of the research discussed in this thesis.

Figure 2.3: A visual representation of the Witteveen research cited in [16]

2.3.3 Levitation of a disc

Laithwaite discusses a setup with currents passing through a set of two oppositely wound concentric coils, which enable stable levitation. The interaction of magnetic fields rising from the two coils will create a stable plane of levitation, as shown in figure 2.4. The coils are represented by cross-sections, while the white portion surrounding the coils is the iron core.

This system was further developed in a similar approach, as referenced in [17]. Ghayoor's system adopts Laithwaite's strategy, and passes current through coils varied at a 180° phase angle. This allows magnetic field lines from the two coils to interact with one another, creating a surface over which the disc can stably levitate.

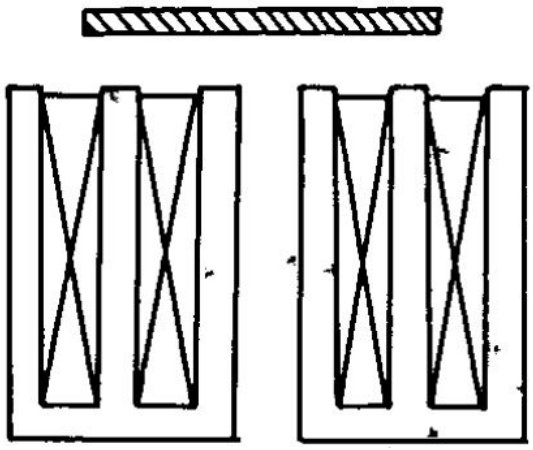

Figure 2.4: A planar section of the system with anti-parallel coils, embedded in an iron core [18]

Using this principle, the coils are designed for this research. There is a requirement of two

concentric coils, anti-parallel to each other, to allow for a stable magnetic field for levitation, as seen in figure 2.5. Along with this, it is highly preferred to use a ferromagnetic material as a core. A ferromagnetic material would have high relative permeability, resulting in densely concentrated magnetic flux passing through the system. A disc is designed for levitation. A multi-purpose power supply is selected allowing for a high-voltage experimentation, along with frequency modulation from 1 - 1000 Hz alternating current. This power supply would also have an in-built controller for voltage control, resulting in an advanced manipulation of disc height above the coils. This is required for the eventual application of this research, in an additive manufacturing environment. Material deposition on top of the disc would cause an increase in weight, as well as alternating impact forces, which could lead to a creation of non-uniform geometries and topologies. This is a highly undesirable characteristic, and hence, disc levitation requires control. The system would also need to be enclosed for high-voltage experimentation. This is done in accordance with CSA guidelines.

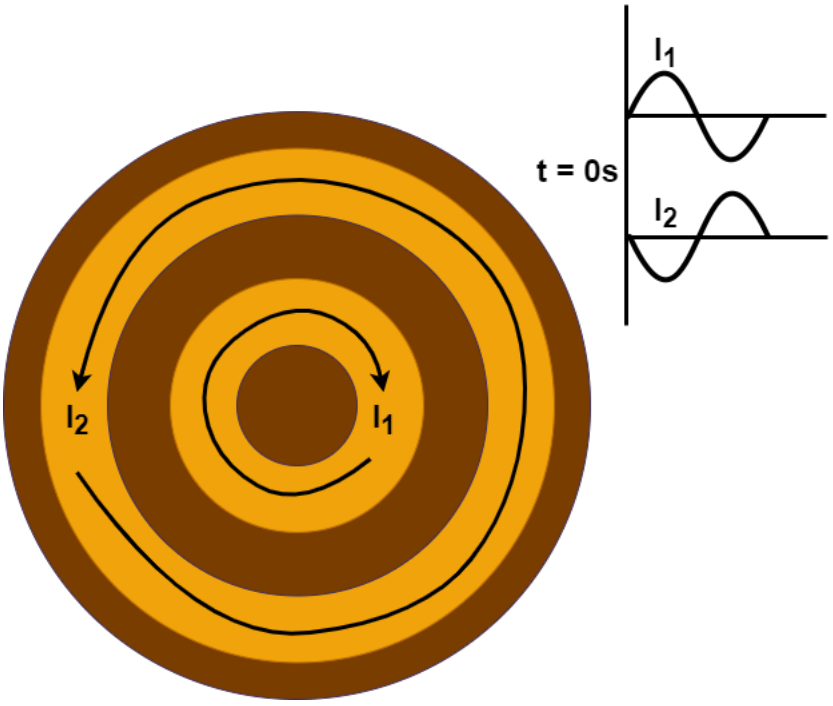

Figure 2.5: TOP VIEW - Intended system for design

Chapter 3

System Design

This chapter discusses the design of the electromagnetic coils for disc levitation for this research. ANSYS Maxwell is selected as the FEMM based software of choice. Three types of analyses namely eddy-current, transient and transient with motion band, are conducted The core material selection is discussed, as it constitutes a major part of the system performance. The optimization technique for achieving the best coil dimensions is explained in detail. Finally, the disc optimization is conducted to achieve the perfect size and material selection for optimal levitation. The manufactured electromagnetic coils are shown in figure 3.1.

Figure 3.1: Manufacutred electromagnetic coils

3.1 Selection of ANSYS Maxwell as a reliable software

ANSYS Maxwell is a FEMM based software which simulates an electromagnetic environment. It is used in design of complex electromagnetic systems such as electric motors, radio frequency antennas, etc. as it provides realistic interpretations of such systems. It is important to validate this software by comparing its output with the observations provided in the experimental work in reference work.

Two reference papers are selected for the purpose of this validation, as cited in [11] and [17].

In [11], the author describes a system consisting of a copper coil wound around an air core. An Aluminum plate is used a base for eddy-current induction, and subsequent magnetic field generation for propulsion of coils. The coils consist of tightly wound 16 AWG wires having 107 turns and are supplied with different currents at 60Hz. The coils are provided with 21A, 26A and 39A RMS to observe levitation heights of 0, 10 and 20mm respectively. ANSYS Maxwell confirms this observation with the active levitation force and position graphs as shown in figure 3.2. Simulation is conducted with an input current of 26A RMS, and steady state levitation height is observed at **10.2mm**, with a net error of **1.96%** compared to [11].

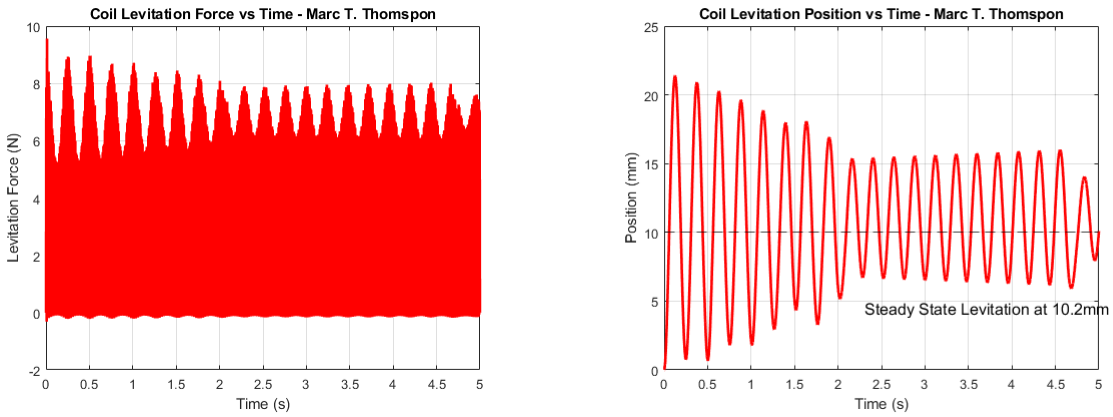

(a) Levitation Force (b) Axial position of coils

Figure 3.2: ANSYS Maxwell validation of Marc T. Thompson's reference paper [11]

The author in [17] shows a system consisting of anti-parallel coils responsible for stable levitation of an aluminum disc. The system consists of 22 AWG wire sets, with the inner coil having 620 turns and the outer coil having 540 turns. Currents of varying magnitudes are passed through the coils at 50Hz. The following response is observed in ANSYS Maxwell, as shown in figure 3.3, while validating the observations of the system. Simulation is conducted

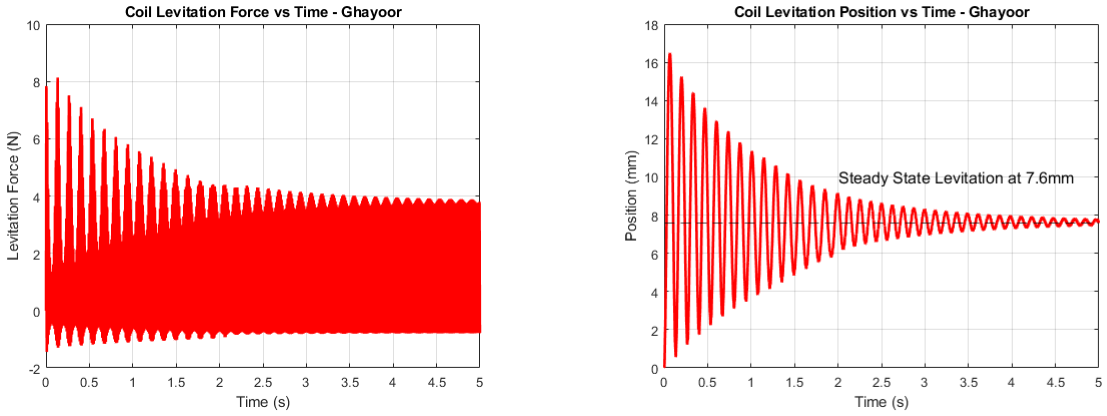

(a) Levitation Force (b) Axial position of disc

Figure 3.3: ANSYS Maxwell validation of Ghayoor's reference paper [17]

with an input current of 2.5A RMS, and steady state levitation height is observed at **7.6mm**, with a net error of **7.89%** compared to [17].

The response curves generated in ANSYS Maxwell are in close agreement with the observations made through real-world experiments, hence validating the use of ANSYS Maxwell for design of coils in this research.

3.2 Setup Design

Coil design is the most important aspect of this research as all aspects such as core design, disc design, and optimization for levitation and restoration forces is conducted based on how efficient the coil design is. Table 3.1 provides a list of initial constraints adopted to give this research a direction. This table has been developed based on the spatial constraints within the additive manufacturing environment, specifically **DMD IC-106** [9].

CONSTRAINTS	GOAL	VALUE
Number of Turns in the primary coil	=	1000
Number of Turns in the secondary coil	$\leq$	1000
Outer diameter of coil setup	=	90 mm
Input current	=	5 A RMS
Frequency of input supply	$\geq$ $\leq$	50 HZ 1000 HZ
Wire gauge	=	18 AWG
Levitated disc dimensions	= =	25mm radius 5mm thickness

Table 3.1: Table of constraints

The geometric upper limit for design of coils for this research is dependent on the working space within the additive manufacturing machine targeted for the research application. The DMD IC-106 machine [9] has a $35cm \times 35cm \times 35cm$ print space. This includes the space used by mobile robotic arms carrying the print nozzles. Moreover, the print environment is filled with an inert Argon gas.

The number of turns in the primary coil is set higher than the number of turns in the secondary coil. Based on the principle of magnetic superposition, the vector fields from the two anti-parallel coils counteract each other. The main function of the primary coil is to facilitate disc levitation, since it produces a majority of the axial component of magnetic field. This is attributed to the fact that the radius of the primary coil is lesser than the secondary coil, and hence, magnetic field density due to the primary coil is higher along

the axis, as seen in figure 3.5. This is further explained in equation 3.1.

$$B = \frac{\mu_o n I}{2(a^2 + z^2)^{\frac{3}{2}}} \tag{3.1}$$

where, B is the magnetic flux density, μ_o is the magnetic permeability of the air/vacuum core, n is the number of coil turns, and a and z are the radial and the axial distance from the coil turns to the point of interest on axis, as seen in figure 3.4. In case of a material core, μ_o is replaced by μ_r, the relative magnetic permeability of that material.

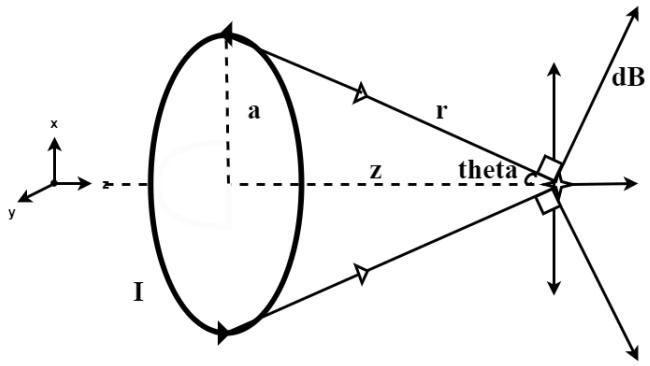

Figure 3.4: Magnetic field at a point on axis of a circular current carrying coil

On the other hand, the main function of the secondary coil is to enable restoration of the disc since it produces a sufficient lateral magnetic flux, compared to its axial component. This is attributed to its outer placement compared to the primary coil, hence, increasing its magnetic field density contribution. This phenomenon can be observed in figure 3.5.

The black arrow represents magnetic field due to the primary coil, and the red arrow

(a) Axial Superposition

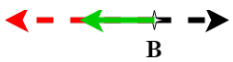

(b) Lateral Superposition

Figure 3.5: Figure a) shows superposition of magnetic fields at a point 'A' imagined along the axis of the coils. Figure b) shows superposition of magnetic fields at a point 'B' imagined off-axis, closer to the secondary coil.

represents magnetic field due to the secondary coil. The green arrow is the superimposed addition of the two vector fields. Figure 3.5a shows superposition of the magnetic field lines due to the primary and secondary coils along the axis. The primary coil has a greater number of turns, and is closer to the axis, than the secondary coil. Assuming the same current is supplied to the two coils, the behavior will be as depicted. The primary coil effect will be greater than the secondary coil effect. On the other hand, the secondary coil is further off-axis than the primary coil. Consequently, upon magnetic superposition, the effect of magnetic field due to the secondary coil will be greater than the primary coil, as shown in figure 3.5b.

An 18 AWG copper wire has a diameter of 1.0237mm. According to [11] [19], the skin depth effect causes the effective resistance of a conductor to increase at higher frequencies of input supply, as shown in figure 3.6. The skin depth is computed as follows:

$$\delta = \frac{1}{\sqrt{\pi f \mu \sigma}} \tag{3.2}$$

where, δ is the skin depth of the material, 'f' is the frequency of the input supply, μ is the permeability of the material, and σ is the conductivity of the material. As evident, the skin depth is inversely proportional to the frequency of input supply. For an 18 AWG copper coil, the skin depth at 1000 Hz is **2.0897 mm**, which is greater than the wire diameter, hence, not affecting the resistance of the system significantly. The skin depth effect changes resistance as follows:

$$R_{AC} = R_{DC} k \sqrt{f} \tag{3.3}$$

where, R_{AC} is the effective resistance due to the skin depth effect, R_{DC} is the characteristic resistance of the coil due to its geometric and material properties, k is a computational factor, and f is the frequency of input supply in megahertz. For coils designed in this research the additional AC resistance will not be significantly impactful to the system, and can be ignored.

3.2.1 Coil Design

Magnetic systems are complex to design. There is sufficient data available on how to design single-coil single-core setups for a specific application.

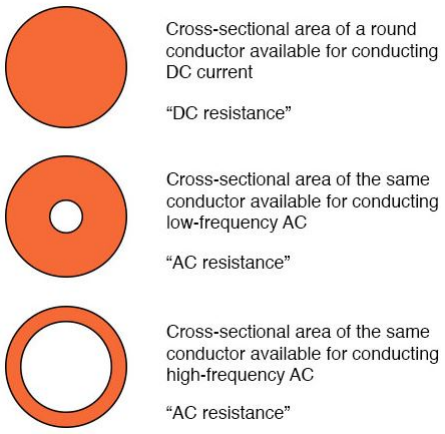

Figure 3.6: Skin depth effect [19]

In reference [20], the author describes a system designed on the basis of power efficiency. A Fabry factor G, as shown in figure 3.7, is developed based on coil geometry ratios, and dimensions are optimized to create a system with the least heat dissipation. This results in the most optimal magnetic field generation, with a G-factor of **0.1792**.

Genetic algorithm has been used to create systems for levitation purposes. In reference [21], the author develops a set of coils to stably levitate a metallic spherical ball. The design of coils involves the usage of a Genetic algorithm optimization technique, were a parent generation is developed, and based on analytical models, upto 60 generations are created using coil loop addition, deletion and reposition methods. The final generation produces the most optimal result.

Finding an optimized coil geometry for a multi-coil multi-core system is a complex task. There are no available resources to provide analytical models for optimization of variables.

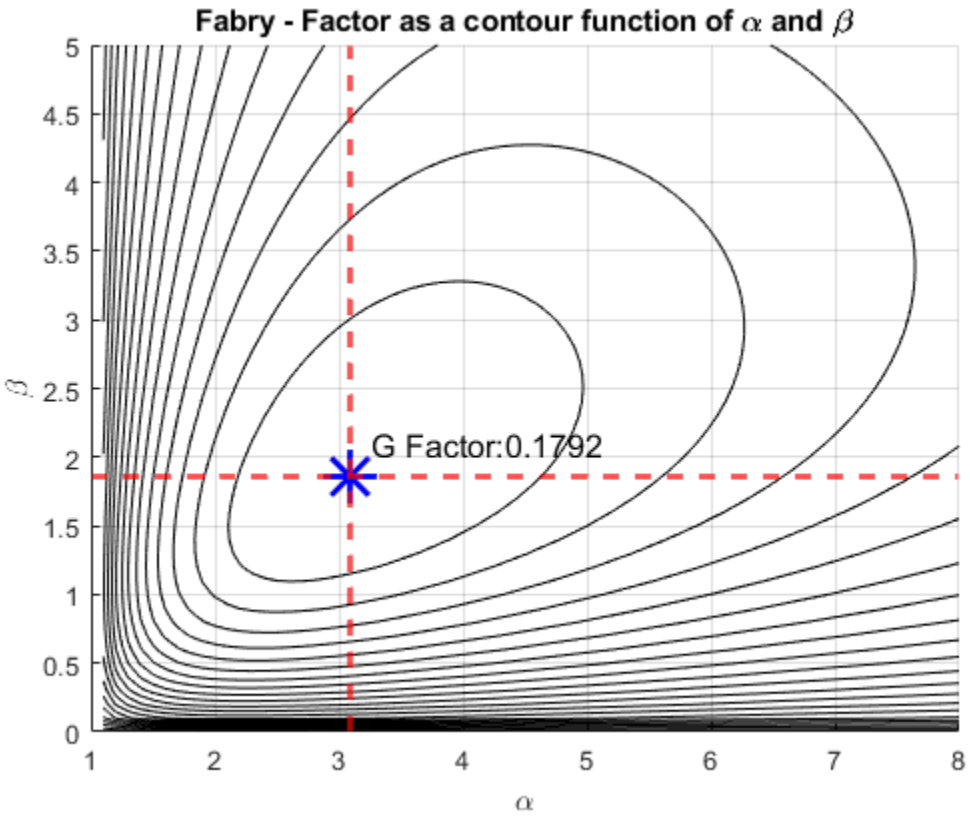

Figure 3.7: G - Factor as a contour function of the geometric properties of the system presented in [20]

As described in earlier sections, ANSYS Maxwell simulations are relied upon to find the desired parameters.ANSYS Maxwell utilizes inputs such as material definition, geometry and dimensioning, orientation of object, power inputs, eddy-current as well as power loss effects and calculates force, torque, inductance and position of disc in levitation. This software has been deemed accurate in simulating real-world electromagnetic behavior.

ANSYS Maxwell is used to create a *dummy model* of the electromagnetic levitation system. Based on systems designed in [18] and [17], the system is provided with component

geometries, and dimensions are kept variable. A 5A RMS 1000Hz input is used, and a parametric sweep of dimensions is performed over a range of values as described in table 3.2.

STEPS	**PARAMETER**	
STEP 1	Inner Coil Width	10mm - 15mm, increments of 1mm
	Outer Coil Width	5mm - 15mm, increments of 1mm
STEP 2	Inner and Outer Coil Placements	Comparing ratios of outer to inner coil placement
STEP 3	Height of Base Core	1mm - 15mm, increments of 1mm

Table 3.2: Parametrization of Coil Dimensions

All systems variations are compared based on the output levitation force on the disc in the axial direction. Restoration force is given a secondary priority here, since this force is expected from the deposition of metal powder during additive manufacturing applications, and it is calculated to be a small value. Coil resistance, inductance and impedance are also noted.

It is to be noted that the parametrization performed to obtain coil dimensions may lead to the acquisition of a local maxima/minima of the aforementioned variables. There is no analytical method available to compute a global maxima/minima of the said values.

Coil Radial Width Optimization

The widths of the inner and outer coil are varied incrementally as mentioned in table 3.2 using ANSYS Maxwell. Figure 3.8 shows the variation trend for the inner and outer coils based on the maximum generated levitation force.

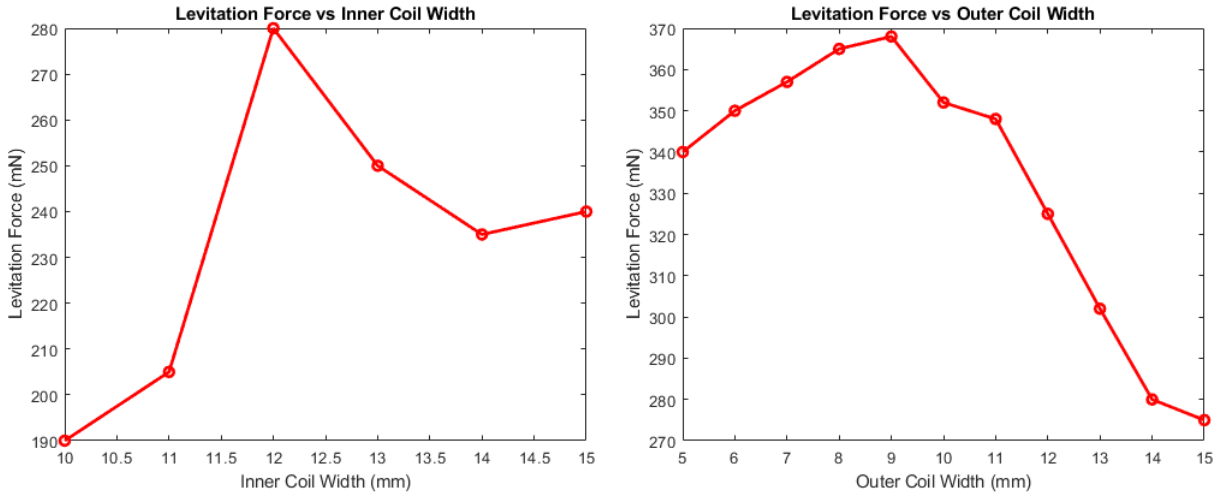

(a) Inner Coil Width Optimization (b) Outer Coil Width Optimization

Figure 3.8: Figure a) shows inner coil width optimization and figure b) shows outer coil width optimization vs levitation force

Coil Radial Placement Optimization

Similarly, the radial placements of the inner and outer coil from the central axis of the coils, are varied incrementally as mentioned in table 3.2 using ANSYS Maxwell. Figure 3.9 shows the variation trend for the levitation force generated by a certain combination of both coils.

Base Core Height Optimization

The relevant literature guiding this research displays systems with a base core. This is because the presence of the base core provides a path of minimal reluctance to the magnetic field lines, causing the flux density to be even higher, and flux lines to be even more compact. Here, reluctance is defined as the magnetic analogue to resistance. It is the opposition

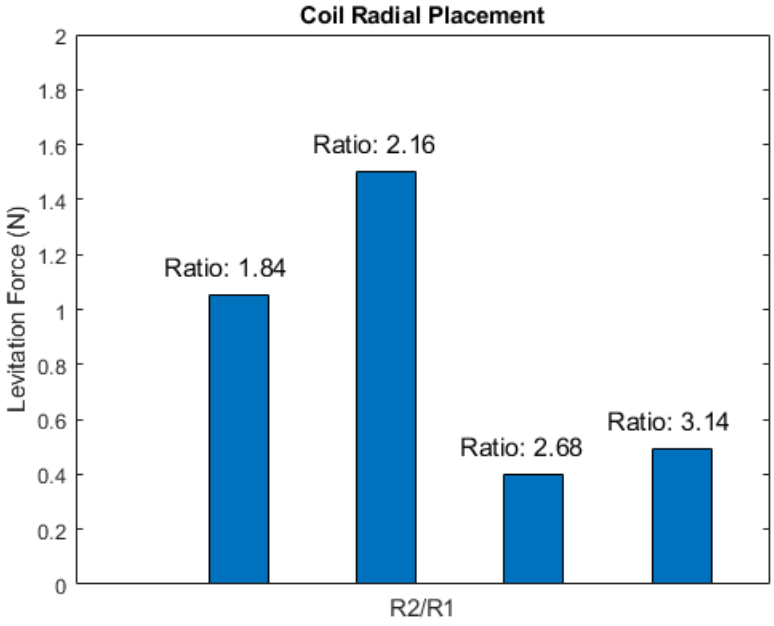

Figure 3.9: Inner and outer coil radial placement shown as a ratio of R2/R1 vs levitation force

offered by a magnetic circuit to the generation of magnetic flux, hence, a path of least reluctance is preferred. Figure 3.10 shows the trends observed in the base core height optimization.

Coil Height

The height of coils is a factor of the number of turns of inner coil, wire gauge and the width of the inner coil. It is also based on the fill factor, which is the ratio of the area of cross-section of the actual number of turns in the coil, to the area of cross-section covered

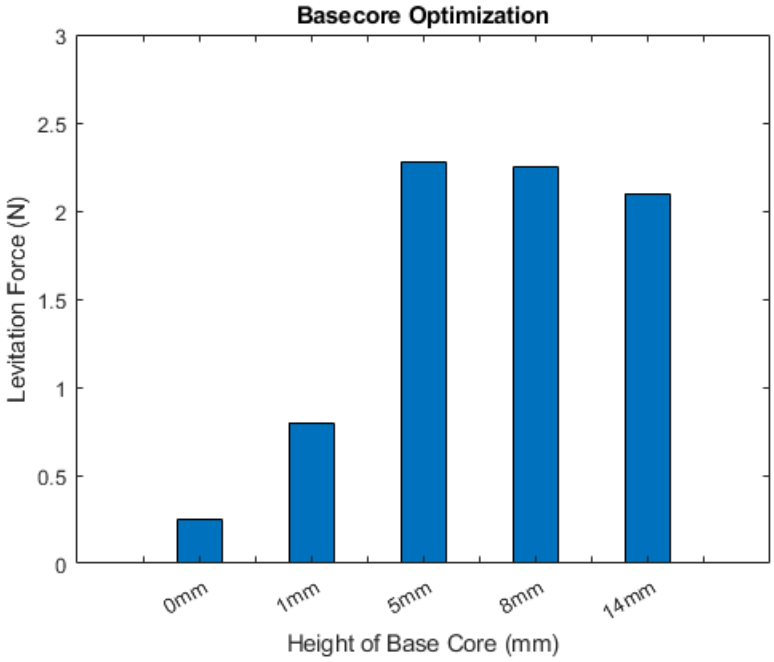

Figure 3.10: Base Core Optimization

by the rectangular ideal inner coil. It is shown in the equation 3.4.

$$FillFactor = \frac{\pi d^2 n}{bh} \tag{3.4}$$

where, n is the number of turns of the coil, d is the 18AWG copper wire diameter, and b and h are the base and height of the rectangular cross-section covered by the coils in a 2-D axis-symmetric view as shown in figure 3.11. The copper wire diameter accounts for insulation, hence, it is input as **1.1mm**. Using a conservative fill factor of **0.72** to account for manufacturing errors, and initial constraint of 1000 turns in the inner coil, the height of the coils is calculated as **110mm**.

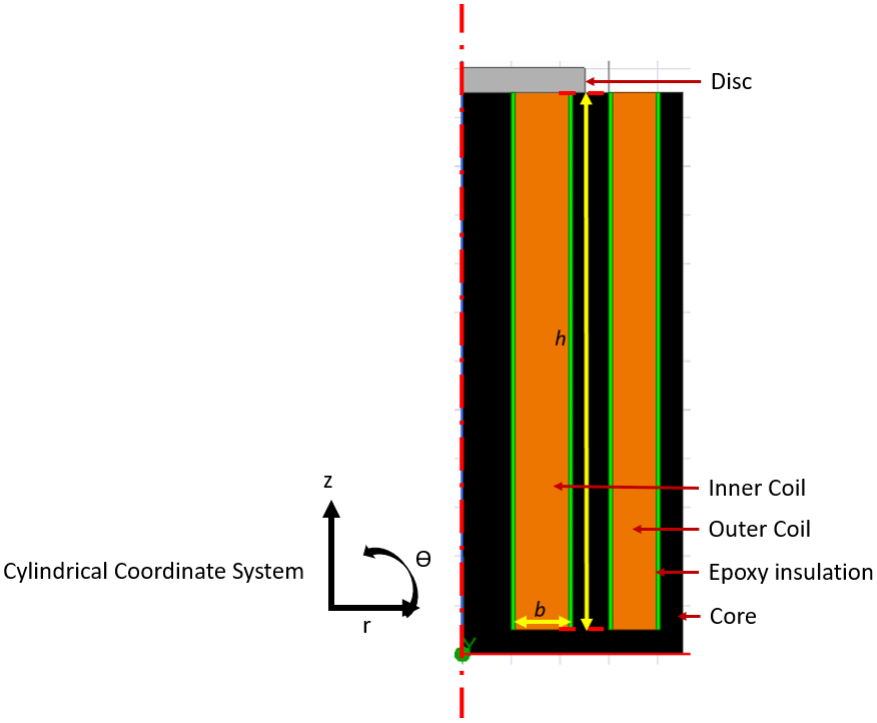

Figure 3.11: 2-D axis-symmetric view of the coils in ANSYS Maxwell

The computed height of 110mm is used to calculate the number of turns of the outer coil as **750 turns**. The finalized coil dimensions are mentioned in the table 3.3.

Adjustment for Coil Manufacturing

From initial parametrization of the system, the number of turns for inner coils is set at 1000 turns, and the outer coil at 750 turns. Some manufacturing errors are encountered during coil winding. Although the initial design for coil dimensions remains the same, the number of turns in the inner and outer coils change. During the theoretical analysis of the system, an 18AWG copper wire is selected, having a diameter of **1.0237mm**. The

DIMENSION	VALUE
Inner Coil Width	12mm
Outer Coil Width	9mm
Inner Coil Placement	10mm
Outer Coil Placement	30mm
Coil Height	110mm
Height of Base core	5mm
Total system height	115mm

Table 3.3: Finalized Coil Dimensions

18AWG copper wires available for manufacturing have an outer diameter of **1.1mm**, hence, allowing for a lesser space to pack 1000 turns. There are two ways to correct and adjust the coil turns to the current system. Case 1 is to maintain the usage of 18AWG copper wire, to supply a peak current of 5A RMS through the coils, by reducing N_1 to 920, and N_2 to 800. Case 2 is to switch to 19AWG copper wire to maintain the initial ratio of $\frac{N_1 I_1}{N_2 I_2}$ as 5:4, with a drawback of reducing the peak current to 3A RMS. ANSYS Maxwell simulations are conducted to compare system performance in both scenarios, as seen in figure 3.12.

$$\text{Strength of coils: Case 1 (Max Amp Capacity: 18 AWG wire)} = \frac{920 \times 5}{800 \times 5} = 1.15 \quad (3.5)$$

$$\text{Net magnetomotive force in Case 1} = (N_1 - N_2) \times 5 = 600 AmpTurns \quad (3.6)$$

$$\text{Strength of coils: Case 2 (Max Amp Capacity: 19 AWG wire)} = \frac{1000 \times 5}{800 \times 5} = 1.25 \quad (3.7)$$

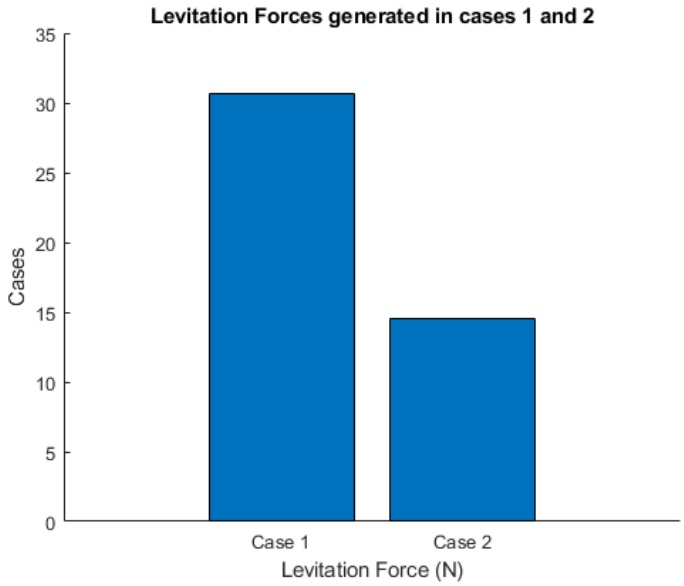

Figure 3.12: Levitation Force comparison between cases 1 and 2 presented in 3.2.1

$$\text{Net magnetomotive force in Case 2} = (N_1 - N_2) \times 3 = 600 AmpTurns \tag{3.8}$$

Despite having a higher strength of coils in case 2, the net magnetomotive force in each case is equal. Additionally, the net inductance, and hence, impedance of the system is lower in case 1, compared to case 2, due to lower number of turns. This explains a higher levitation force generated in case 1, compared to case 2, as seen in 3.12. Therefore, the corrected number of turns for the inner coils is modified to **920 turns**. The outer coil is corrected to **800 turns**.

3.2.2 Core selection

Electrodynamic suspension of a paramagnetic object requires a high concentration of magnetic flux passing through the coils. Higher the concentration of magnetic flux, higher

the magnetic field density. This is essential as the levitation force on the disc is portrayed as shown in equation 3.9.

$$F_{lev} = J \times B \tag{3.9}$$

where, J stands for the eddy current density induced through the disc. Since J is a factor of material property of the disc, hence, a high magnetic field density is required in conjunction with J for a good levitation. Core selection is essential for a robust magnetic field density B.

As mentioned in equation 3.1, the magnetic field density is directly proportional to the permeability of the selected core. The relative permeability is defined as follows:

$$\mu_r = \frac{\mu}{\mu_o} \tag{3.10}$$

where, μ_r is defined as the ratio of the absolute permeability μ of the material, to permeability of free space μ_o.

Ferromagnetic materials such as pure iron, ferrite and electric steel have a high relative permeability, thus they are selected and compared in performance to see the optimal levitation force generation.

The levitation and restoration forces generated by each material are varied over current ranging from 1A RMS to 5A RMS, as shown in figures 3.13a and 3.13b

As levitation forces constitute the primary importance of design objectives, pure iron is

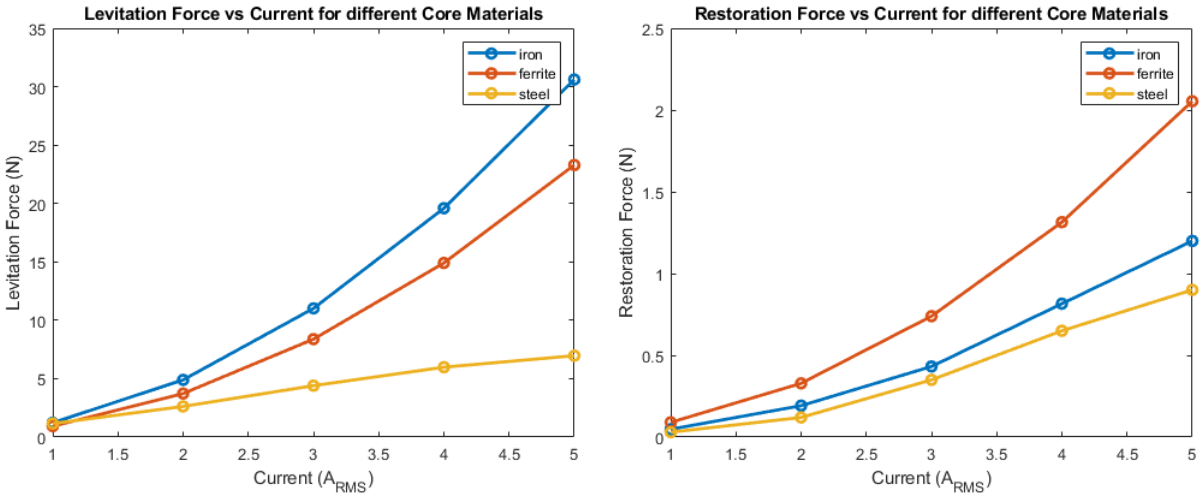

(a) Levitation Force vs Current for different core materials at 1000Hz

(b) Restoration Force vs Current for different core materials at 1000Hz

Figure 3.13: Comparison of different materials

picked as core material, due to the higer levitation forces generated by it. Ferrite produces better restoration forces than pure iron, but restoration is secondary in hierarchy of decision making for core selection. The restoration forces generated by all materials are high enough in general to restore the disc laterally.

3.2.3 Disc Design

Disc Material

As mentioned in the previous section, according to equation 3.9, the levitation force on the disc is a factor of the material property of the disc. Current density J varies as mentioned in equation 3.11.

$$J = E_{induced}\sigma \tag{3.11}$$

where, $E_{induced}$ represents the induced EMF through the disc, and σ is the electrical conductivity of the disc. Aluminum has a high conductivity of 3.8×10^9 Siemens per meter, and an extremely low density of 2710 kg per m^3. This implies that the levitated object made of Aluminum can stay light, while highly conducting. Thus, Aluminum has a high levitation ability, hence, it is chosen for this research.

Disc Size

Disc radii ranging from 10mm to 60mm, and heights ranging from 1mm to 10mm are compared to obtain the optimal size for the maximum levitation force. Similar to coil design, the restoration force is not prioritized, and is a secondary point of concern. This optimization is performed over a range of input frequencies, 50Hz - 1000Hz. This is shown in figure 3.14

Evidently, a disc radius of 25mm, and disc height of 5mm produces the optimal levitation forces; it is chosen as the disc size.

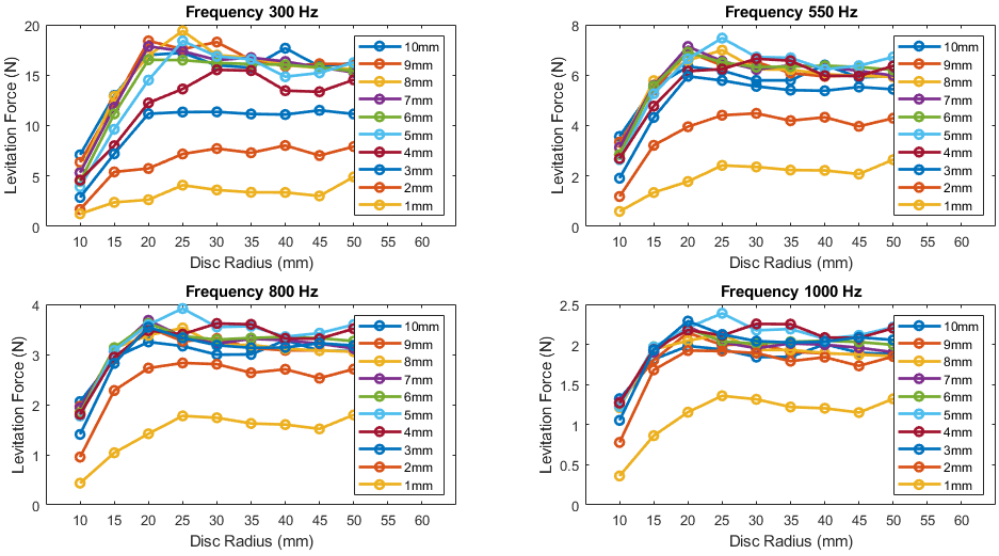

Figure 3.14: Disc Levitation forces as a function of radii and heights, at various frequencies

Chapter 4

Thermal Analysis

This chapter discusses the thermal analysis conducted for the electromagnetic (EM) coils. This system consists of a solid pure iron core which is prone to EM losses. As the temperature of the coils increases over time, the overall current reduces due to the increase in DC resistance. It may also damage the epoxy resin holding the coils in place. The losses from the coils and the core are modelled in ANSYS Workbench's Mechanical environment and a worst-case measure is discussed.

4.1 Necessity for Thermal Analysis

4.1.1 Coil DC Resistance

The 18AWG copper wires used in winding the coils for this electromagnetic levitation setup have a total DC resistance of 5.814Ω. According to [22], the resistance of a copper coil

varies with temperature according to the following formula:

$$R_f = R_i \frac{(T_f + 234.5)}{(T_i + 234.5)} \tag{4.1}$$

Where, R_i stands for initial resistance of the coils, R_f stands for the final resistance after a certain operating time, T_i is the initial ambient temperature, and T_f is the final temperature of the coils leading to an increase in resistance. An increase in temperature and a subsequent increase in resistance of coils would lead to a reduction in the overall current. The variation of resistance with temperature and the following change current with resistance can be seen in the figure 4.1.

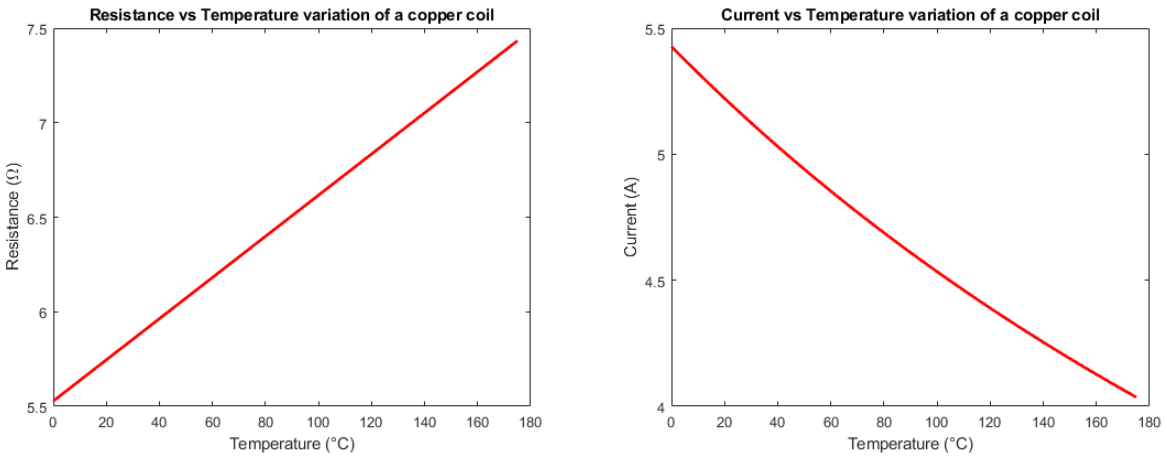

(a) Variation of resistance with temperature (b) Variation of current with temperature

Figure 4.1: Variation of Resistance and Current with Temperature

4.1.2 Effect of Temperature on Core Permeability

The pure iron material used for core manufacturing has a steady relative permeability of 9400 in the linear region of its B-H curve, explained in greater detail in chapter 6. As temperature of the core rises up to 700 °C, the permeability remains fairly steady, but beyond the critical temperature of 776 °C, the core becomes practically non-magnetic, as referenced in [23]. This is because as temperature rises, the inter-molecular forces weaken and they get more and more aligned towards the direction of magnetization. This effect is not as pronounced as the oscillations of the molecular magnets, which occur in the opposing direction to their alignment, and completely oppose the magnetizing ability of the material above the critical temperature. This can be better visualized through figure 4.2.

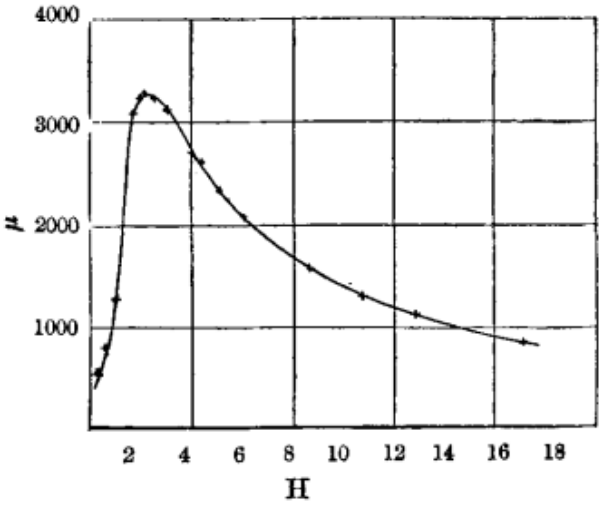

Figure 4.2: Variation of permeability of iron with temperature [23]

4.1.3 Epoxy Protection

The materials used in the manufacturing of coils, namely copper (melting temperature = 1083 °C [24]) and iron (melting temperature = 1538 °C [25]) have a higher melting point than epoxy. Therefore, the thermal analysis is limited to inspection for melting point of epoxy. The coils require the use of an epoxy resin to hold the wires inside an insulating environment. This ensures that the wires experience no contact with the core or other coils and prevents and shorting. The guide to operating temperature for the epoxy used for these coils indicates a maximum of 180 °C as referenced in [26]. The coils are expected to stay under the prescribed maximum limit to minimize epoxy damage. This makes the need for a thermal analysis even more important.

4.2 System Thermals

The electromagnetic coil setup is a complex RL circuit where the coils are designed to support contact less levitation of a disc. Although the inductance of the coils has a significant impact on the net current and the subsequent force of levitation generated by the system, it has no effect on the net power losses. The major components of this system responsible for power losses are:

- The resistive element in the copper coils
- The solid pure iron core

4.2.1 Coil Thermals

The system circuit can be represented as seen in figure 4.3:

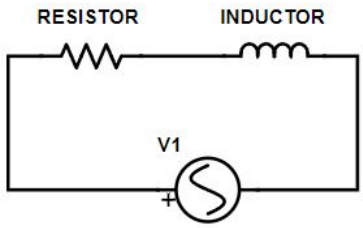

Figure 4.3: Circuit Diagram

As evident, the two major components of the circuit are the resistive and the inductive elements. Figure 4.4 shows the variation of net power consumed by each element in a circuit as current flows through them upon application of a voltage. Figure 4.4a shows that the entirety of the input power from the source supply gets consumed and lost through the resistive element as heat, and is referred to as 'real power', referenced in [27]. Here, the phase angle difference between the voltage and current waveforms is 0 °. On the contrary, figure 4.4b shows that as voltage and its current, lagging at a 90 °phase angle difference, flow through the circuit, the net power consumed in one half of the cycle is entirely returned to the power source, hence, there is no net power loss.

In an RL circuit like the electromagnetic coils presented in this research, there is a variation in the aforementioned behavior as the two elements work together in the system. Figure 4.5 shows the DC resistance, inductive reactance and the net phase angle difference in this system.

According to [27], the net power consumed due to the resistive element in the circuit

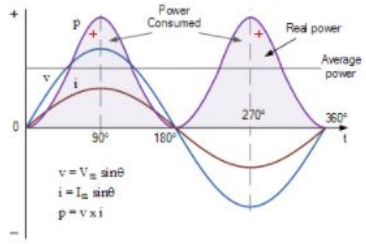

(a) Power loss from a resistive element

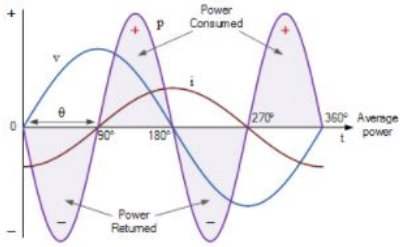

(b) Power loss from an inductive element

Figure 4.4: Figure a) shows the net power loss from a resistive element in a purely resisitve circuit, whereas figure b) the net power loss and return from an indcuctive element in a purely inductive circuit

can be represented through the following equation:

$$P_{loss} = VI\cos\theta \tag{4.2}$$

Where, θ is the phase angle difference between the voltage and the current wave forms. Hence, the net computed power loss from the coils is **182.73 W**.

4.2.2 Core Thermals

The electromagnetic core is a major component in contributing to the overall losses in the system. Although it is difficult to predict core losses under transient conditions from magnetic devices, such as inductors, transformers, and other e-machines, some approaches have been developed as mentioned in [28]. The overall power loss from a core can be represented as follows:

$$P_v = P_h + P_c + P_e = k_h f {B_m}^{\beta} + k_c f {B_m}^2 + k_e f {B_m}^{1.5} \tag{4.3}$$

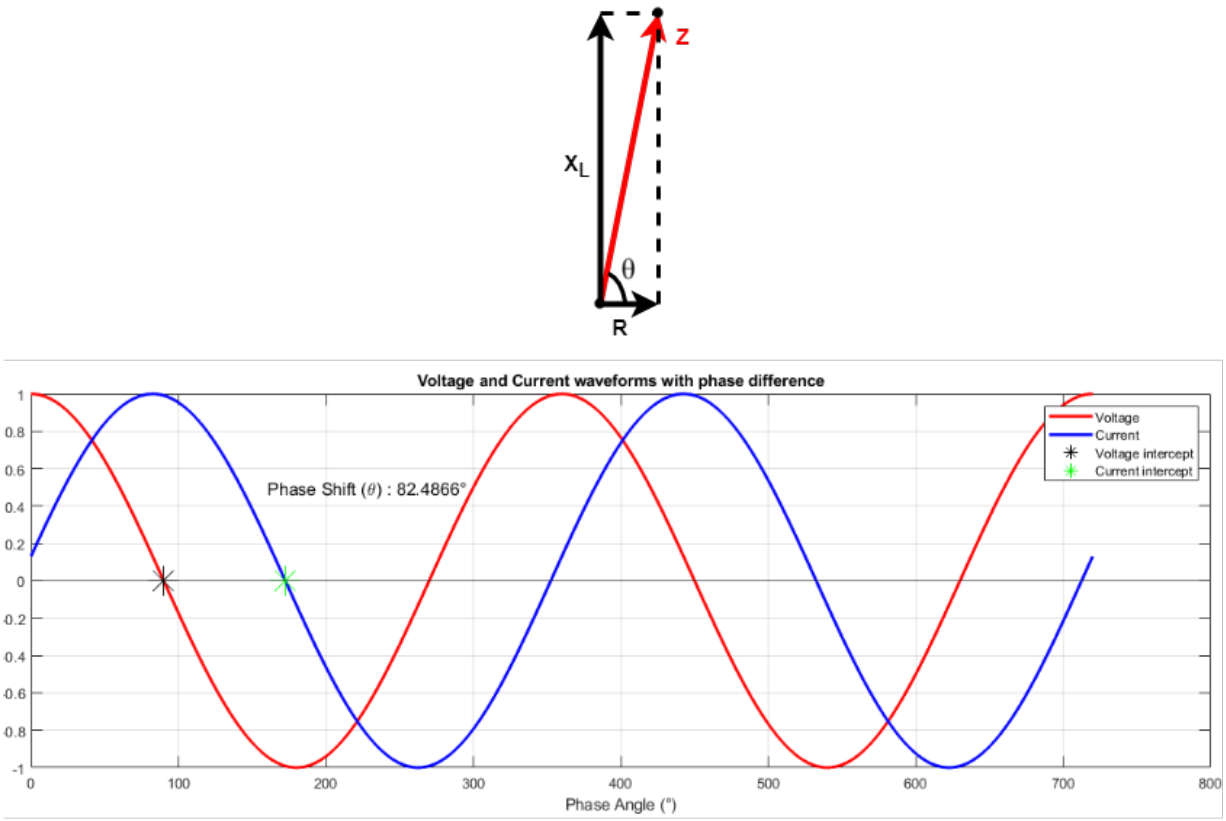

Figure 4.5: Phasor diagram and, voltage and current waveforms with phase shift for these electromagnetic coils. Phasor diagram not to scale

where, P_v is the volumetric core power loss, P_c is the eddy current loss, P_h is the hysteresis loss and P_e amounts to excess losses. The k_c, k_h, k_c, and parameter β are used to compute the net power loss per unit volume. In the time domain, the computation of eddy current losses and excess losses is easier, but hysteresis losses are difficult to calculate. Hence, an empirical model known as the 'Steinmetz equation' is widely used for ferrite-based cores. For sinusoidal inputs, the equation is represented as follows:

$$P_v = C_m f^{\alpha} \Delta B^{\beta} \tag{4.4}$$

Where, C_m is the loss constant, α is the frequency exponent and β is the magnetic flux density exponent.

The core material used in this project is a solid pure iron core. The material properties of the core are discussed in greater detail in chapter 6. The core is assumed to have a power ferrite core model. According to [29] the values for Cm, α and β can be assumed as seen in table 4.1:

PROPERTY	VALUE
C_m	3.397
α	1.979
β	2.628

Table 4.1: Power Ferrite Core loss model properties

ANSYS Maxwell material properties are modified to support this setting. The net core loss is computed to be **176W**.

4.3 Net System Loss

The net power loss computed through the coils and the iron core are further used to compute the temperature variation of the system. As mentioned in the earlier sections, the temperature of the coils can lead to a higher DC resistance, therefore lower current, and can also damage the epoxy, which may lead to shorting. ANSYS Workbench's Mechanical

environment is used to conduct a transient thermal analysis for 20 mins of heat generation. The specified time constraint is considered sufficient to replicate the system performance during a 20-minute additive manufacturing activity. The coil and core components are input with their corresponding losses, and temperature of the entire system is visualized as seen in figure 4.6. This variation is further plotted vs time in figure 4.7.

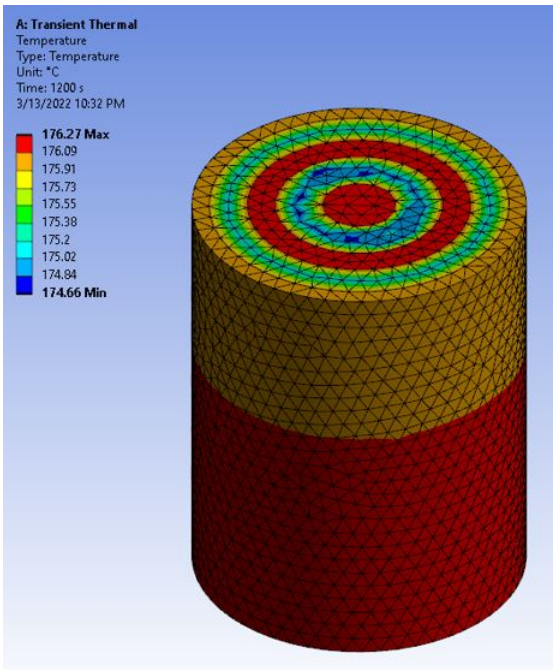

Figure 4.6: Temperature contour of system after 20 minutes of operation

The maximum temperature of the system is mostly constituted around the outer core, reaching up to **176°C**. This temperature is a worst case measure. projected to be achieved after 20 minutes of constant operation at 300V RMS, 85Hz. This is a simulated upper limit of temperature, and is below the conservative melting point of epoxy as mentioned in subsection 4.1.3. This temperature is also much lower than the critical temperature of demagnetization of the iron core, as reflected in subsection 4.1.2. Therefore, it is safe to

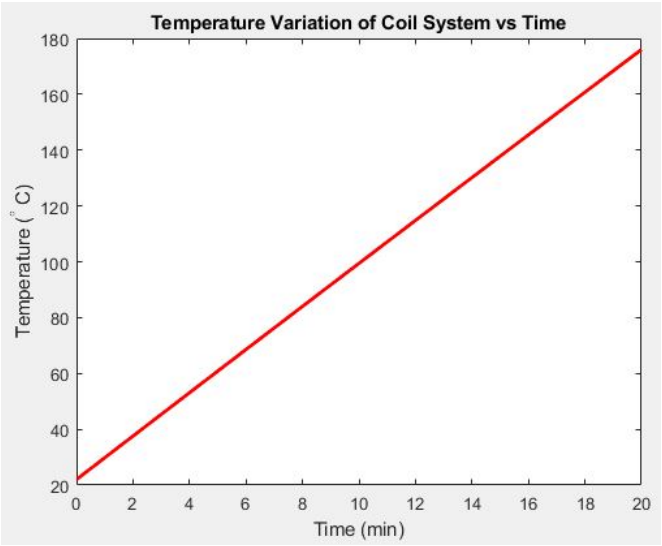

Figure 4.7: Temperature variation of system over 20 minutes of operation

assume that the system can function without failure.

4.4 Disc Thermals

A similar approach is applied to analyze the temperature vs time variation for the selected Aluminum disc. Aluminum has a melting point of 660 °C [30], thus, the temperature of the disc is ensured to be well under this limit after 20 minutes.

Aluminum, unlike the iron core, has a majority of its power loss in the form of eddy current losses. As current is induced in the aluminum disc, due to an external magnetic field, it flows throughout the volume of the disc in a concentric manner. A current density plot created for a 2D cross-section of half the disc shows that the current generation through the disc is non-uniform. A majority of the current flows through the outer part of the disc

as seen in figure 4.8. This can also be attributed to the skin-depth action of the material, as explained in detail in chapter 3.

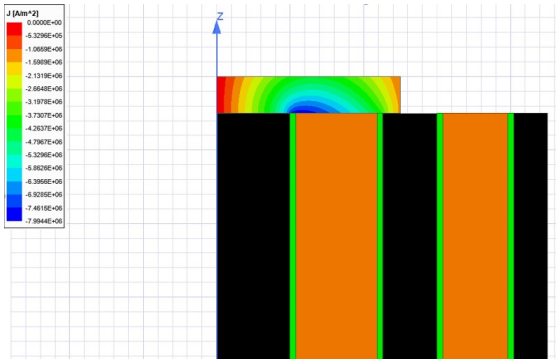

Figure 4.8: Current Density plot of a 2D axis-symmetric cross-section of half the disc

The average losses from the disc are nearly **8W**. This is due to the high conductivity of Aluminum. Eddy current losses are emitted from the disc in the form of heat. Therefore, a temperature plot of disc is plotted over 20 minutes of operation. This can be seen in figures 4.9 and 4.10.

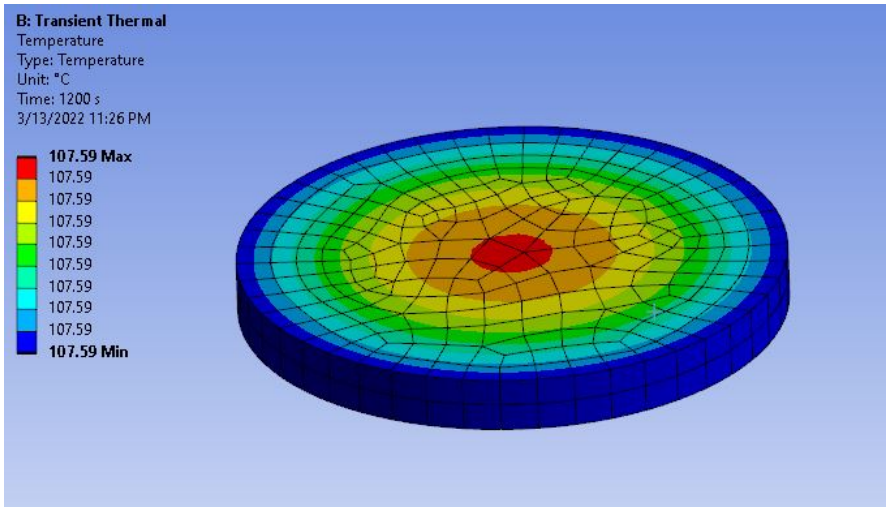

Figure 4.9: Temperature contour of the disc after 20 minutes

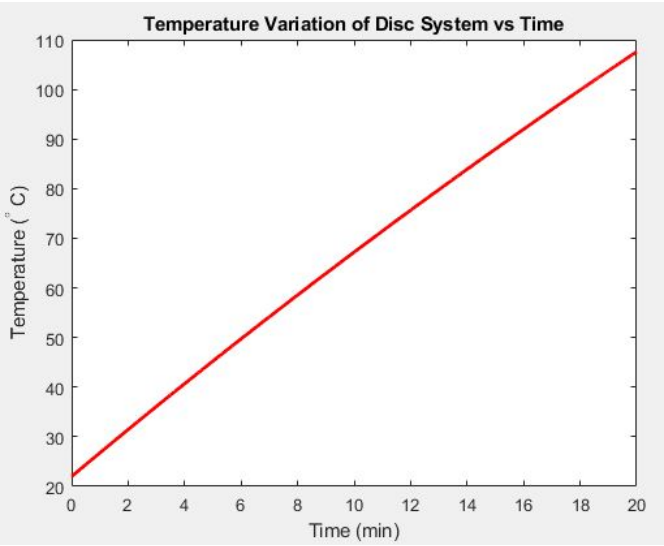

Figure 4.10: Temperature variation of disc over 20 minutes of operation

As evident, the maximum temperature of the disc after 20 minutes of operation is **107°C**. This is well below the melting temperature of Aluminum as mentioned in this section, hence, levitation of the disc for 20 minutes will not have any counteracting effects.

It must be noted that the thermal analysis conducted for this system is to provide a conservative upper limit to temperature. The system is simulated to operate at 5A RMS passing through both coils for 20 minutes leading to a rise in temperature up to 176 °C. For successful levitation of disc, as explained in chapter 6, the current through the inner coil is **4.65A RMS** and current through outer coil is **2.78A RMS**, which will significantly bring the temperature of system after 20 minutes of operation down to a lower degree. A possible cooling mechanism is also discussed in the section labeled as 'Future Work' in chapter 7.

Chapter 5

Experimental Setup

This chapter describes the use of selected hardware with fabricated coils. A heavy-duty power supply is used to conduct low-voltage and high-voltage experiments to understand real-world behavior of the magnetic field and current produced in the coils, as well as their correlation with ANSYS Maxwell simulations. Since the system is complex, basic methods cannot be used to predict coil inductance and subsequent impedance. Two techniques are used to predict coil inductance - a series resonant frequency analysis for minimum impedance, and a time constant analysis. These are compared with the solution from ANSYS Maxwell. Finally, an enclosure is created according to CSA guidelines, to eventually obtain CSA certification and approval, for use in an additive manufacturing environment. An overall experimental setup schematic is shown in figure 5.1.

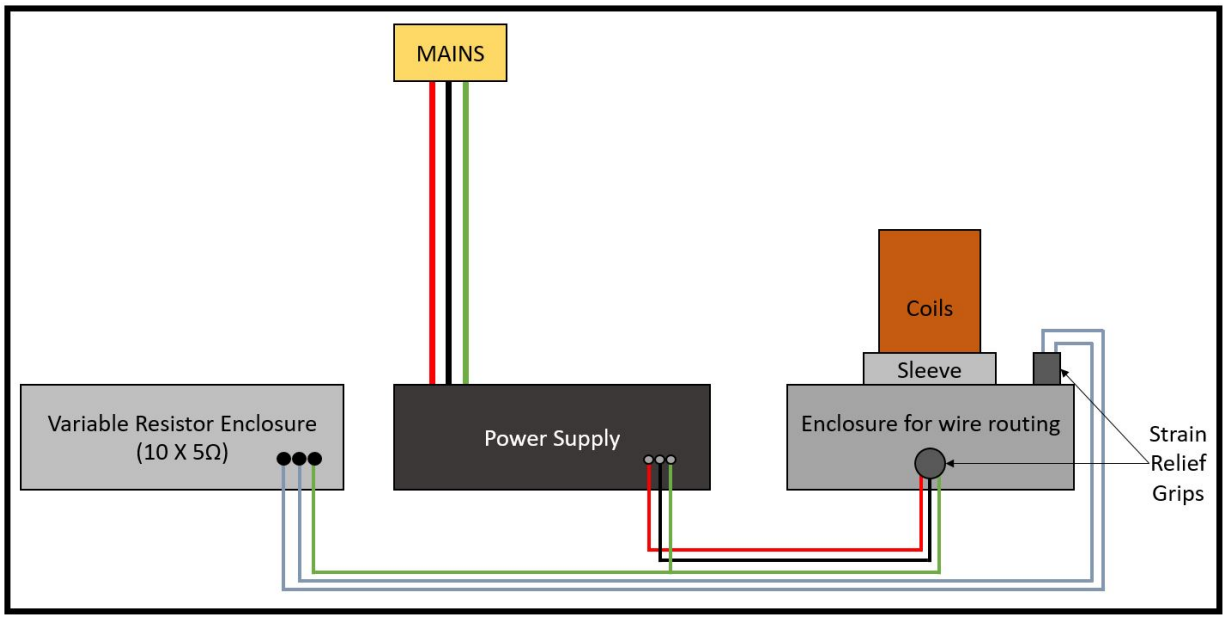

Figure 5.1: Experimental setup schematic

5.1 Hardware Selection

The different kinds of hardware used in this research are listed as follows:

- Power supply with capability of supplying high voltages up to 1000Hz input frequency
- Gaussmeter with a high resolution
- Oscilloscope with a high resolution
- Current clamp compatible with the oscilloscope

Figure 5.2: BK Precision 9832B Power Supply

5.1.1 Power Supply Selection

Based on the constraints mentioned in earlier sections, hardware selection was tailored to finding a power supply capable of supplying a high performance, low total harmonic distortion input wave to the coils. BK Precision 9832B, seen in figure 5.2, was selected for the same, as it can supply AC, DC, and AC + DC waves of sinusoidal, square, and custom nature. Additionally, this power supply is equipped with an in-built rectifier-inverter-transformer circuit, in conjunction to a proprietary controller. The 9832B power supply has a capability to supply up to 2kW power in AC or DC forms. A 300V RMS potential difference can be applied across a load, to extract a maximum of 10A RMS, which is a necessity for this electromagnetic system, as the impedance is observed to be high. A key emphasis in selection of this power supply was placed on its ability to supply output voltage waveforms ranging from 45 – 1200Hz, thus fitting the constraints mentioned in earlier sections. The coils portray strong inductive load behavior; therefore, this power supply is deemed suitable as it possesses a high output current crest factor, along with low input resistance.

Safety is of prime importance since this system runs on high power electricity, hence hardware compliance with CSA (Canadian Standards Association) approval is top priority. The SPE-1000 certification is model code for one-time approvals of custom electric products being used in Canada, and it falls under the CSA guidelines. The 9832B power supply is SPE-1000 certified.

5.1.2 Gaussmeter selection

Measurement of magnetic field requires a fast, high-resolution machine with repeatable flux density measurement capability. The Lakeshore 421 Gaussmeter was selected for this purpose. It is paired with the MNA-1904-VH axial probe consisting of a hall effect sensor at its tip. This probe can accurately calculate AC RMS and DC magnetic fields ranging from 30 Gauss to 30 kGauss (or 3 Tesla).

The coils produce magnetic fields less than 1 Tesla at maximum current capacity at the axial tip of the system, thus confirming the suitability of the probe and gaussmeter.

5.1.3 Oscilloscope and Current Sensor

BK Precision 2567 Oscilloscope is deemed appropriate for this research as it has a high resolution of up to 200MHz. The measurement of voltage and current can be performed simultaneously as this device has 4 channels for concurrent measurements. This is necessary for computing phase difference between voltage and current waveforms during inductance measurement. The oscilloscope can measure at least 400V pk which is beneficial for this research, as the peak voltage for high power experiments is 424V pk (or 300V RMS).

Maximum current measurement capability is well beyond the peak allowable current for 18AWG copper wires.

The BK Precision CP62 current clamp compliments the oscilloscope as it can measure up to 100A RMS, sufficient for the application of this research.

5.2 Low-Voltage Experiments

The electromagnetic coils were connected to the power supply to conduct low-voltage experiments. This was done to study the coils' current response and magnetic field generation. The impedance of the coils is expected to be high, hence, it is important to study performance of coils at 50Hz and 1000Hz.

Two types of experiments were conducted – coils in series with 0 degrees phase difference, and coils in series with 180 degrees phase difference. A potential difference ranging from 5V RMS to 20V RMS was supplied at 50Hz and 1000Hz to understand coil characteristics. The following image shows variation of current with voltage in all cases. This is compared with ANSYS Maxwell simulations as shown in figure 5.3

As observed, the error between experimental and simulation results is minimal, hence, the results are acceptable. The experimental calculation of coil impedance in either case is in line with ANSYS Maxwell computations. Evidently, the current and magnetic field density is much higher for the 50Hz input than in the case of 1000Hz. This makes a case to move ahead with using 50Hz for disc levitation. This current can further be increased by using a capacitor in series with the coils.

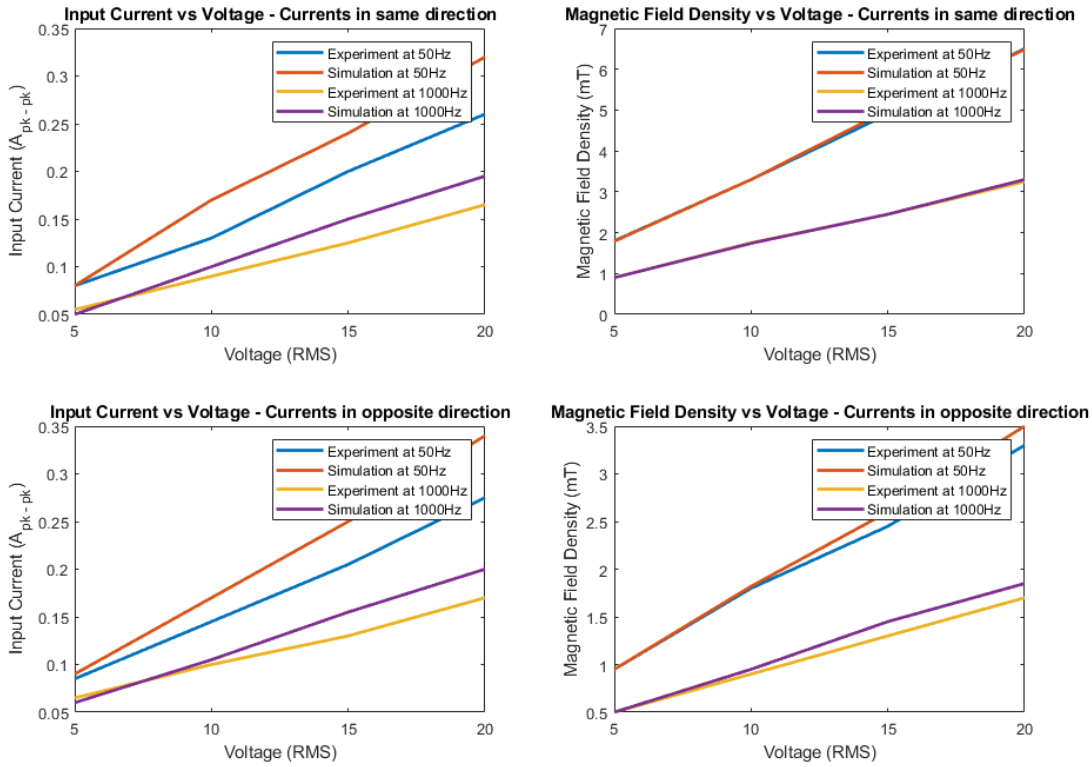

Figure 5.3: Current vs Voltage, Magnetic Field Density comparison at 50Hz and 1000Hz: Experiments and Simulations

5.3 High-Voltage Experiments

The emphasis is then shifted to high-voltage experiments. Since the electromagnetic coils have complex characteristics, contrary to initial belief, a non-linear relation is observed while conducting Ohm's law test. For this experiment, a potential difference ranging from 100V RMS to 300V RMS is applied across the coils. The magnetic field is measured on the axial tip of the coils, and current is measured at 50Hz.

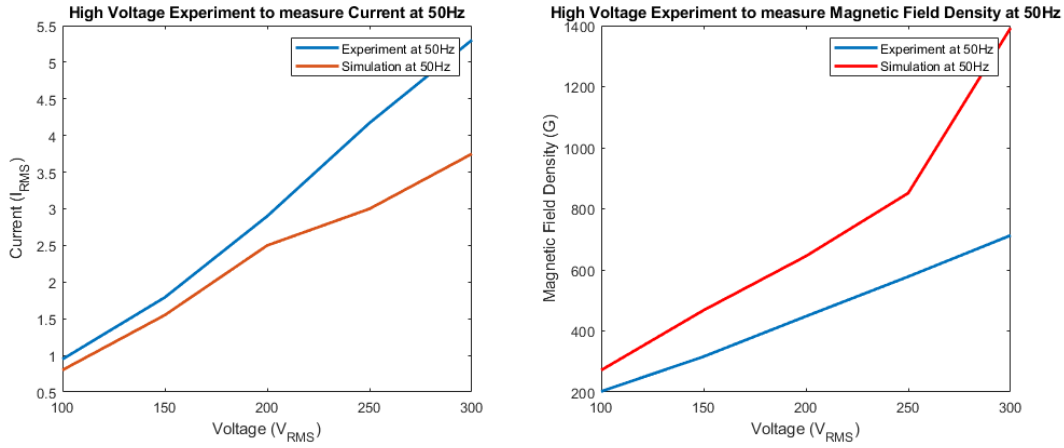

Figure 5.4: Current vs Voltage, Magnetic Field Density comparison at 50Hz: Experiments and Simulations

As evident from figure 5.4, there is significant discrepancy between current and magnetic field measurement at high voltages across the two test cases. This indicates a diversion from expected behavior from simulations. The reason is based on the intrinsic properties of the electromagnetic coils, such as relative permeability and inductance. This is further inspected in section 6.2. This also indicates that calculation of inductance of coils using analytical methods is a complex task and measuring inductance using experiments is the optimal way to go.

5.4 Inductance Measurement

Inductance is an intrinsic property of any electromagnetic coil system. It is a tendency of a system to oppose the change of current passing through it. It depends on factors such as the relative permeability of the core-coil system and the number of turns. For any system, having a higher inductance is beneficial as magnetic field density is directly proportional to

inductance.

$$L = \frac{N\Phi}{I} = \frac{NBA}{I}, L \propto B \tag{5.1}$$

where, Φ is the magnetic flux, A is the area of cross-section through which flux lines pass, and B is the magnetic fiend density. Despite its major advantage, inductance also creates a counteractive effect on the performance of the system. In electromagnetic systems using an AC supply, the frequency of the input wave, in conjunction with inductance of the coils, creates inductive reactance, which is the AC analogue of resistance offered to current flow through coils.

$$X_L = 2\pi f L \tag{5.2}$$

where, X_L is the inductive reactance, f is the input frequency, and L is the inductance of the coils. The higher the frequency of input supply, for a certain inductance, the higher the inductive reactance. The impedance of an AC system is defined as follows:

$$Z = \sqrt{R^2 + (X_L - X_C)^2} \tag{5.3}$$

where, X_L is the inductive reactance, and X_C is the capacitive reactance. It is assumed that the intrinsic parasitic capacitance of the system is minimal, hence its counter impact on the performance of the system is ignored. The higher the inductive reactance of the system, the lower the overall current passing through the system, the worse the performance. This

makes calculation of inductance a highly essential aspect of analyzing an electromagnetic system.

As mentioned in the earlier section, this electromagnetic system is complex, as it consists of multiple coils and multiple cores. Several techniques have been employed to calculate inductance of single coil, single core systems, using analytical models. As mentioned in [31] a rectangular cross-section of the coils can be assumed to estimate the inductance of an electromagnetic system using the following equation:

$$L_o = Fn^2d - \frac{0.03193n^2ac}{b}(0.693 + B_s)microhenrys \tag{5.4}$$

where, L_o is the nominal inductance of the coils with an air core, n is the number of turns of the coils, F and B_s are geometric factors, and a, b, c and d are geometric dimensions of the coils shown in figure 5.5.

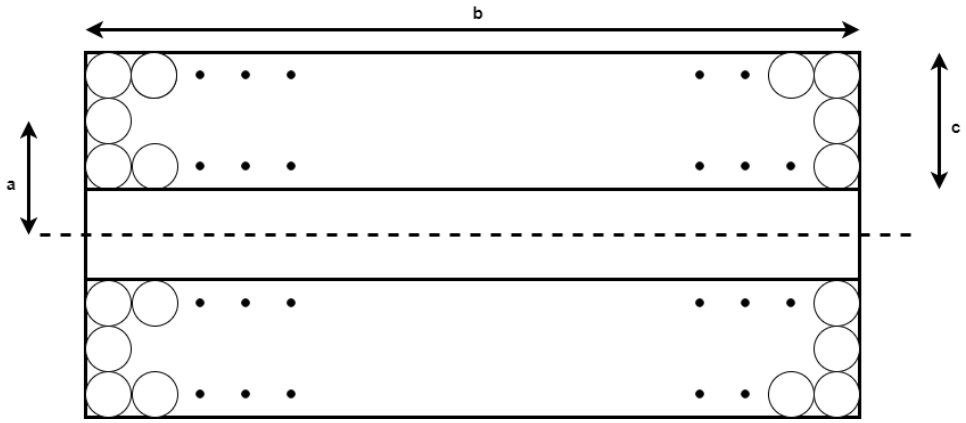

Figure 5.5: Long multiple-layer coil

Unlike the above stated model, the coils in this system have a complex mutual inductance,

which is difficult to estimate because of multiple concentric axial cores. No references have been found to successfully calculate inductance of a complex electromagnetic system.

Estimating inductance through experimental methods is the optimal way to solve this problem. Two methods are employed to measure inductance of the coils. These methods are tailored to an electromagnetic RLC (Resistance – Inductance – Capacitance) circuit. A series resonant frequency analysis, and a time constant analysis are conducted.

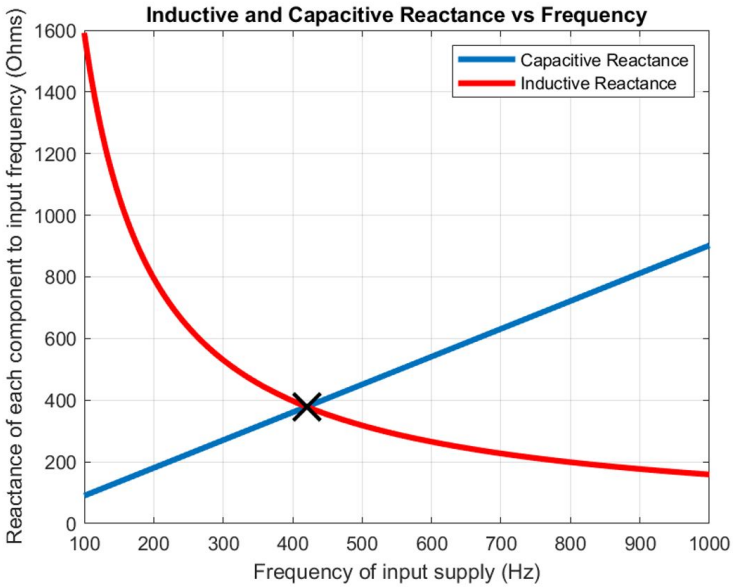

Figure 5.6: At 420Hz, the inductive and capacitive reactances negate each other's effects. Hence, Z = R, and L = 0.1436H

5.4.1 Series resonant frequency

The parasitic capacitance of this system is assumed to be parallel in connection to the coils, which can be best shown through an RLC (Resistor – Inductor – Capacitor) circuit. This electromagnetic system can be considered as a tank circuit, where the capacitor is in parallel

with the coils. Here, the parasitic capacitance of the coils is ignored, as it is calculated to be 23.66pF which will have minimal effect on the coil characteristics. A capacitor is connected in series to the coils to create an RLC circuit. The current passing through a series RLC circuit is maximum at the resonant frequency. Alternately, the impedance of this system is lowest at the resonant frequency. Based on the following equation, the inductive and capacitive reactance of the system counteract and negate the effect of each other at the resonant frequency as mentioned in equation 5.5.

$$X_L = X_C \tag{5.5}$$

$$2\pi f_{resonance} L = \frac{1}{2\pi f_{resonance} C} \tag{5.6}$$

$$f_{resonance} = \frac{1}{2\pi\sqrt{LC}} \tag{5.7}$$

For this experiment a 1uF capacitor is considered suitable for connection in series with the coils. A 10V peak-to-peak sine wave is supplied through the system. The current is measured to be **1.21A RMS** at an input supply of 420Hz. This is deemed as the resonant frequency of the series RLC circuit.

To support this validation, the time difference between the current and voltage wave forms is observed to be $20\mu s$, which computes to a net phase difference of 3.024° which is very small. This further confirms that resonance has been achieved as capacitive reactance

completely negates the effect of inductive reactance. This can be seen in figure 5.7

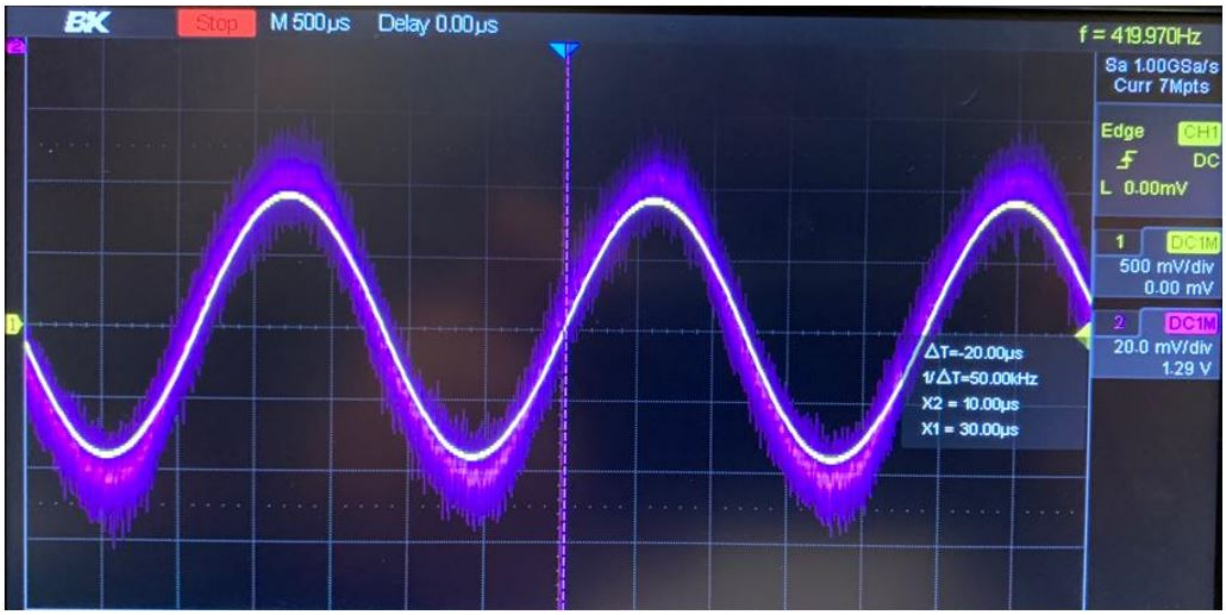

Figure 5.7: At 420Hz, the votlage and current waveforms overlap each other with a $20\mu s$ (or 3.024°) shift

5.4.2 Time Constant Experiment

The time constant of an RL (Resistor – Inductor) circuit is the measure of time taken by the system to achieve a steady state peak current upon application of a potential difference across its components. It is defined as follows:

Evidently, it is calculated as the time taken by the system to rise from its initial value to **63.2%** of its peak value. As mentioned in the previous section, the parasitic capacitance is calculated to be almost negligible (23.66pF). Effects of its capacitive reactance can be ignored at low frequencies as it is in parallel to the coils.

A 2Ω sandstone resistor is connected in series with the circuit as shown in fig. A voltage of 3V RMS square wave is applied across the circuit at 1Hz input frequency. The peak steady-state current $I_o$is recorded as **0.52A RMS**. Consequently, time taken to achieve 63.2% $I_o$is measured using the oscilloscope. Time constant is measured as **18.00ms** as shown in figure 5.8

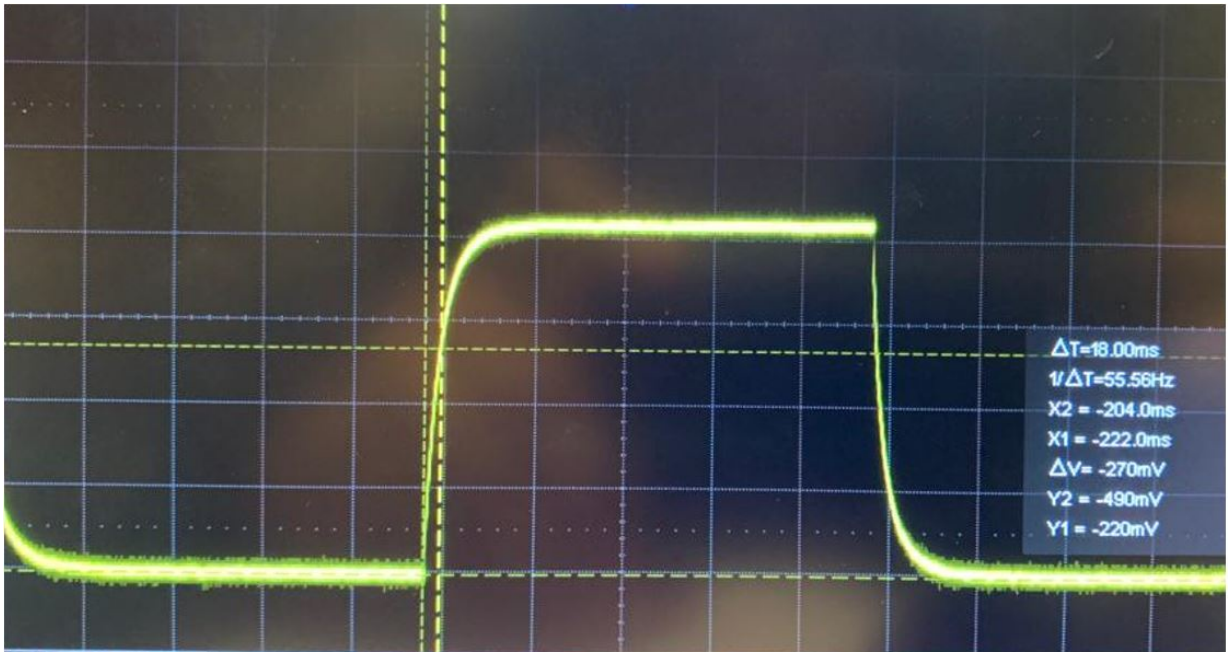

Figure 5.8: Step response of the current

Inductance is calculated as **0.1404H**.

5.4.3 ANSYS Maxwell Matrix Inductance

ANSYS Maxwell calculates inductance using a Finite Element approach. The entire system is converted into a matrix of characteristics such as materials and dimensions, based on

the number of mesh elements used. The electromagnetic system is converted into 31195 mesh elements with a maximum edge length of 4.56mm for optimal accuracy. Inductance of coils is calculated by system matrix as **0.13598H**. Inductance calculated from the three techniques is compared in table 5.1, and average inductance is calculated.

TECHNIQUE	INDUCTANCE (mH)	NET ERROR (max - min)
Series Resonance Frequency	143.6	5.32 %
Time Constant Experiment	140.4	
ANSYS Maxwell	135.96	
Average Inductance	139.98	

Table 5.1: Inductance

The net error between maximum and minimum values is computed to be **5.3%**, which is deemed appropriately low.

5.5 Enclosure construction for AM environment compatibility

The experimentation in this research is conducted at extremely high voltages. The output power from the power supply is protected against over voltage and over current supply as mentioned in [32]. Despite this, CSA guidelines are closely followed, and any experimentation above 30V RMS or 100W RMS is conducted such that all exposed wires from the system are surrounded by a non-conducting enclosure.

A simple rectangular enclosure is developed as shown in figure 5.9. High-impact resistant

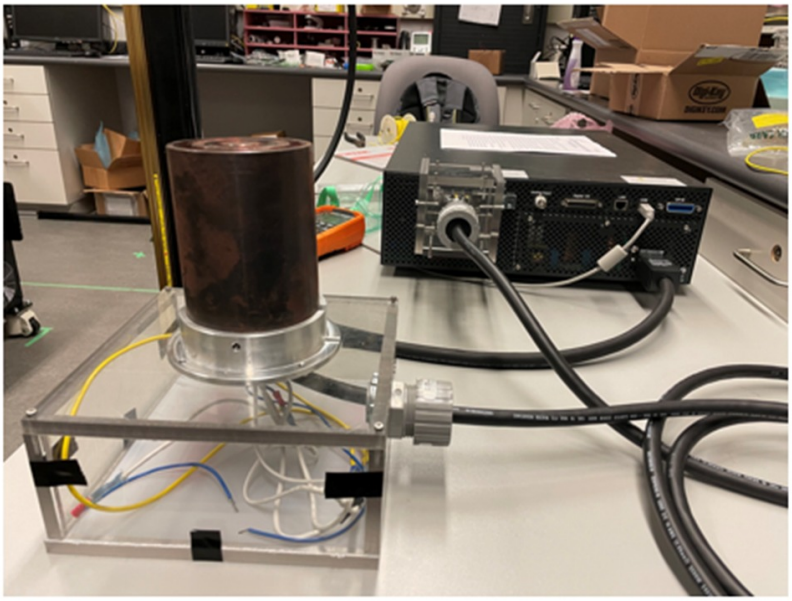

Figure 5.9: Coils on top of the built enclosure

polycarbonate sheets with a Rockwell R118 level hardness, and an impact strength up to 65MPa are used to develop the walls of this enclosure. They possess thermal resistance from $-40°F$ to $180°F$. The material is insulating in nature, hence provides good protection against any live exposed wires. Since the coils in this electromagnetic system are quite heavy, the sheet thickness is selected to be 3/8 inches, or 9.525mm. A deformation analysis is conducted using SolidWorks to validate selection of material.

As evident from figure 5.10, the maximum deformation of the polycarbonate sheet is **0.0104mm**, thus confirming suitability of material.

An Aluminum sleeve is used to house the coils. High-strength strain relief grips are used to grip the electric cables connecting all components in the system. Insulated 3-wire electric cables are used to make connections while grounding the overall system. All connections

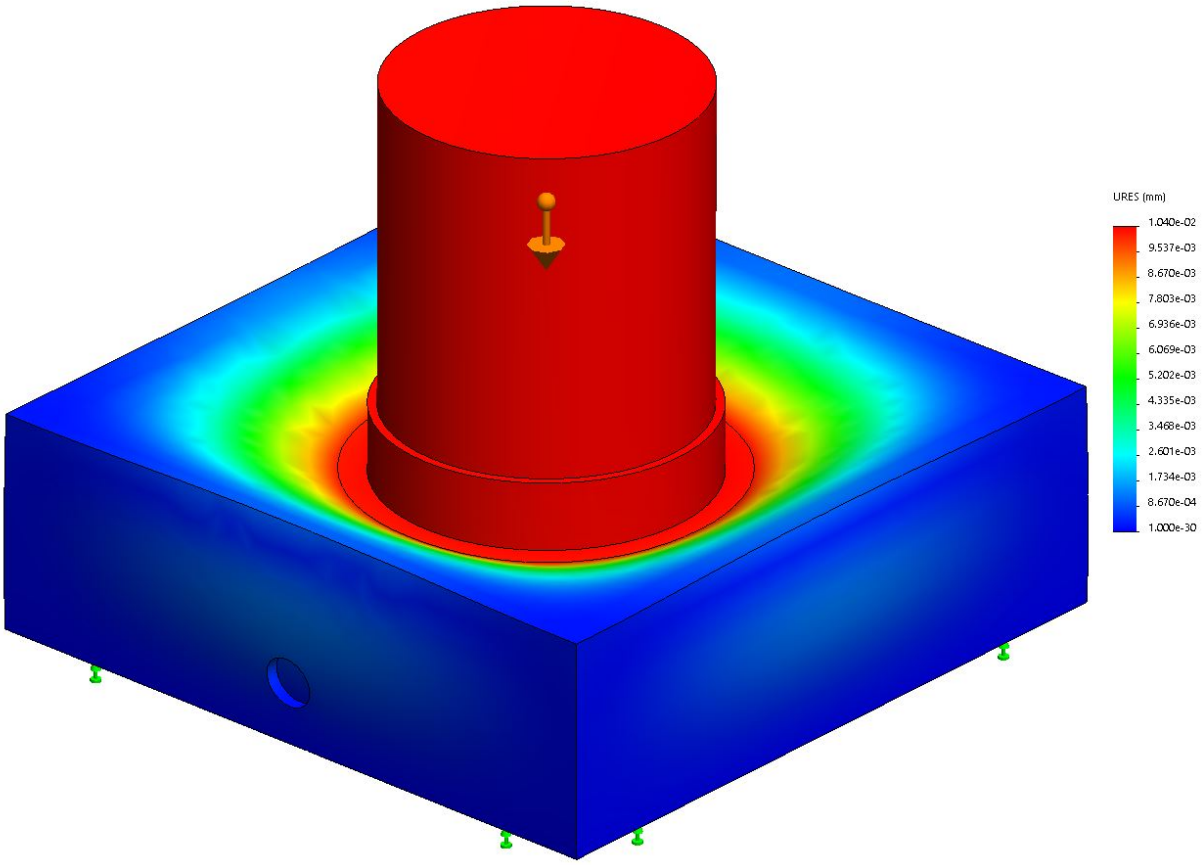

Figure 5.10: Deformation response of the enclosure under the weight of the coils

are made using robust end-to-end electrical male and female butt connectors.

Chapter 6

Electrical Calibration

This chapter explains the deviations observed in the electromagnetic system compared to expected behavior. The limitation of using a 2kW power supply, in addition to using 18 AWG copper wires which can safely supply up to 7A RMS, creates tradeoff issues which are solved using an innovative 'current split' method. The net magnetomotive force (MMF) of coils is maximized, and strength of coils is manually controlled using resistors in parallel. Levitation of disc is observed at 85Hz. Its ability to successfully levitate a payload on top of the Aluminum disc is also noted.

6.1 Levitation Attempts at 50Hz and 1000Hz

The electromagnetic levitation system presented in this research is shown to function at 50Hz and 1000Hz AC input frequencies. Due to intrinsic coil characteristics such as high and inductance, as well as core losses, the performance of the experimental setup differs

from the ANSYS Maxwell simulation results. The system is set up to attempt levitation at 50Hz and 1000Hz.

6.1.1 Levitation at 50Hz

The power supply is used to supply 300V RMS at 50Hz to the electromagnetic coils. As mentioned in section 6.2, according to ANSYS Maxwell simulations, the permeability of the core is expected to be in the linear region of its B-H curve. Due to discrepancies, no proper levitation is observed. The disc vibrates on top of the coils, as seen in6.3. An interesting point to be noted is, that the magnetomotive force of the coils, at 300V RMS and 50Hz, results in a strong restorative force behavior. Hence, if some power can be shifted from the restorative to the levitative coil, a tradeoff can be created, as discussed further in 6.3.1.

6.1.2 Levitation at 1000Hz

At 1000Hz, due to the the high inductance of the system, the net impedance amounts to 879.6ω. Due to the complex behavior of the coils, the inductive reactance is not canceled out by the presence of a capacitor in series with the coils. Hence, the current observed at this frequency is extremely low (approximately 0.34A RMS). This leads to a generation of a low amount of magnetic field density, hence, no levitation is observed.

In both cases it is evident that the generation of axial levitation force is not sufficient to lift the disc. Severe vibrations are observed in the disc indicating one or more of the following possibilities:

- The generation of axial magnetic field is not sufficient to induce significant eddy

currents in the disc. This is more probable as the core selected for this operation is solid, and not laminated, leading to core losses, hysteresis losses, eddy current losses, etc. Another reason is that the core is made of pure iron in which the linear portion of the B-H curve is acquired upon having a strong input magnetomotive force (product of number of turns of coil and current passing through it). This is studied in greater detail in further sections.

- The generation of eddy currents in the disc is not sufficient to induce an opposing axial magnetic field.

6.2 Magnetic Permeability Calibration

High voltage experiments were conducted to measure magnetic field density at the axial tip of electromagnetic coils. The table 6.1 compares the experimental magnetic field density with values obtained from ANSYS Maxwell simulations.

VOLTAGE	EXPERIMENTS (Gauss)	SIMULATIONS (Gauss)	ERROR PERCENTAGE (%)
100	202	271.6	25.6259
150	316	467.8	32.4498
200	448	645	30.5426
250	578	851.54	32.123
300	713	1392.4	48.7935

Table 6.1: Magnetic Field Density at the tip of coils: Experiments vs Simulations

Evidently, the magnetic field density values have significant error in measurement. ANSYS Maxwell has calculates very high values at the tip of the coils. This indicates that

ANSYS Maxwell calculations are performed differently than the active behavior of core and coils. ANSYS Maxwell material selection for the pure iron core shows a constant relative permeability of 9400 as shown in figure 6.1.

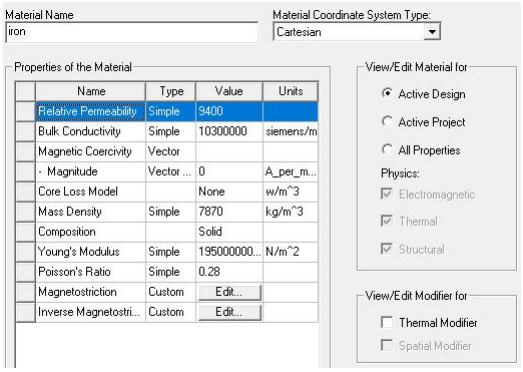

Figure 6.1: ANSYS Maxwell using iron core with a relative permeability of 9400

The core selected for this research is a Low-Carbon magnetic pure iron ASTM A 848-01 with the following B-H curve obtained from the supplier as shown in figure 6.2.

The relative magnetic permeability of a material is calculated as a ratio of its magnetic flux density B and its magnetic field strength H as shown in the following equation:

$$\mu_r = \frac{B}{H} \tag{6.1}$$

The pure iron core consists of a B-H curve with its ideal capability realized in its linear region as shown in the blue portion of the curve. Based on the observations, using trial

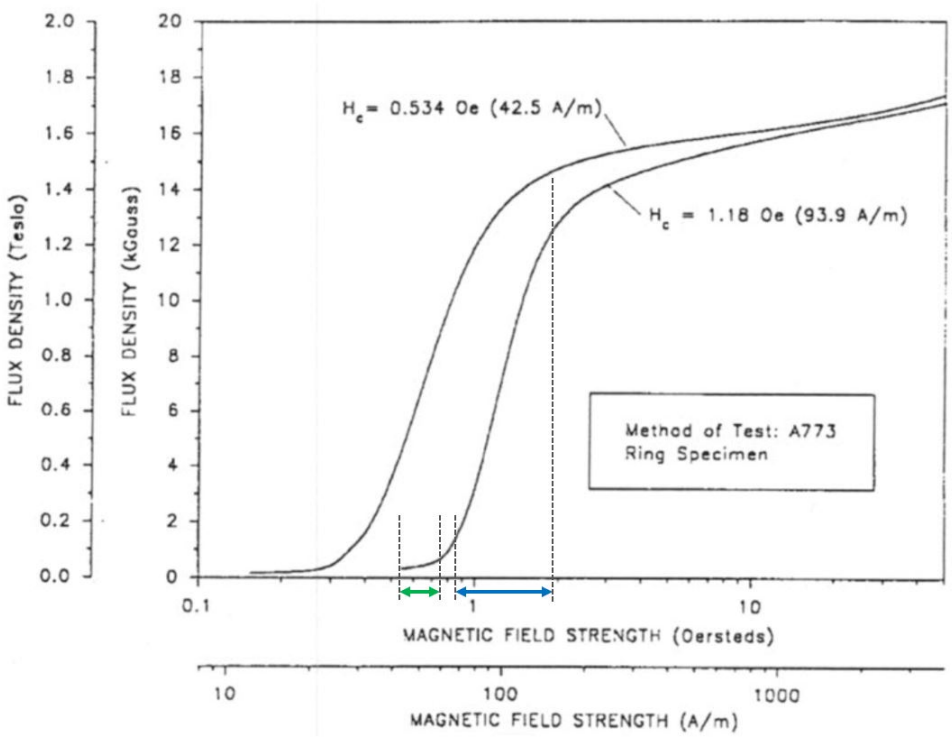

Figure 6.2: The B-H curve of the pure iron core as obtained from the supplier. The green portion of the curve is where this system functions, the blue portion of the curve is the ideal linear region

and error, different permeability values are calculated from the green portion of the curve, and used as input in ANSYS Maxwell to correlate with experimental observations. These observations can be seen in table 6.2.

A relative permeability of 700 was calculated as the active permeability for experimental correlation. This behavior is noted based on the following reasons:

- The inductance of coils is high, leading to high impedance even at a relatively low frequency of input supply. This causes the overall current to reduce, leading to a low

PERMEABILITY	MAGNETIC FIELD DENSITY (Gauss)	ERROR PERCENTAGE (%)
125	335.64	-113.3238
353	414.19	-72.8675
700	**761.556**	**5.9820**
900	805.949	11.1606
1000	831.474	13.8879

Table 6.2: Magnetic Field Density at the tip of coils at 300V, 50Hz: Simulations with different core permeabilities. Error percentages are in comparison with experimental observations

magnetic field generation, and subsequent low magnetic field density.

- The core used for this research is solid and not laminated. This causes significant electromagnetic losses such as eddy current loss and hysteresis loss. These contribute to the overall opposing magnetic field generation, which reduce the net magnetic field produced by the coils.

The input voltage and resultant magnetic field density values of the system are compared with minimal error between experiments and ANSYS Maxwell. The same approach is followed for the magnetic field measurements as shown in the table 6.3.

A solid pure iron core with a relative permeability of 700 shows no levitation in disc, mostly observed as vibratory perturbations as observed through experiments, as seen in figure 6.3

The experimental levitative ability is realized and corrected through strength of coil modifications as mentioned in the following section 6.3.

VOLTAGE (V RMS)	MAGNETIC FIELD DENSITY (Gauss)	ERROR PERCENTAGE (%)
100	215.45	6.24
150	329.45	4.08
200	460.42	2.7
250	591.47	2.28
300	761.556	5.9820

Table 6.3: Magnetic Field Density at the tip of coils: Simulations with different input voltages. Error percentages are in comparison with experimental observations

6.3 Strength of Coils – Magnetomotive Force

A notable feature of levitation attempts for disc at 50Hz and 1000Hz input supply of a 300V RMS sinusoidal voltage is that despite minimal levitation observed, the disc portrays a strong lateral restorative behavior. Figure 6.4 shows a manual external force applied on the disc in lateral directions, and its subsequent restoration to its point of origin.

This indicates a stronger outer coil restorative effect on coils, than the inner coil levitation effect. This behavior is further studied as strength of coils are analyzed and modified.

6.3.1 Trade-off between levitation and restoration – analytical model

Magnetomotive force (MMF) [33] is a measure of coils' ability to push magnetic flux through its circuit. It is depicted as shown in the following equation:

$$MMF = NI \tag{6.2}$$

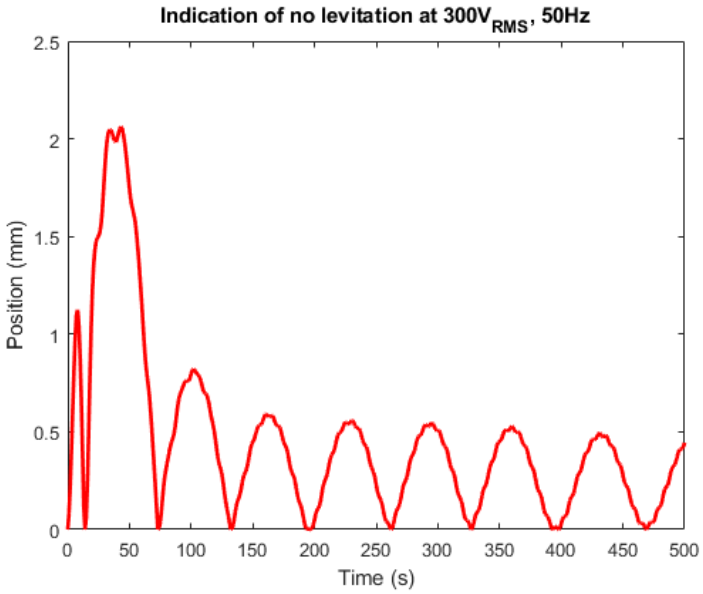

Figure 6.3: Indication of no levitation at 300V RMS, 50Hz with the current strength of coils

where, 'N' is the number of turns, and 'I' is the current passing through the coils. The magnetomotive force of the original electromagnetic system is mentioned in equation 3.6. An electromagnetic levitation setup's ability to levitate objects is dependent on its net magnetomotive force. As mentioned in [17], the average force of levitation produced by a set of concentric coils wound out of phase is depicted as:

$$F_{Zavg} = \frac{(N_1 - N_2)^2 I_o^2 \mu_o A_{airgap}}{4z^2} \tag{6.3}$$

where, N1 and N2 are number of coils of inner and outer coils respectively I_o is the peak amplitude of current flowing through the coils, μ_o is the permeability of free space, A_{airgap} is the area of the air gap under the disc and z is the vertical distance of the disc from the

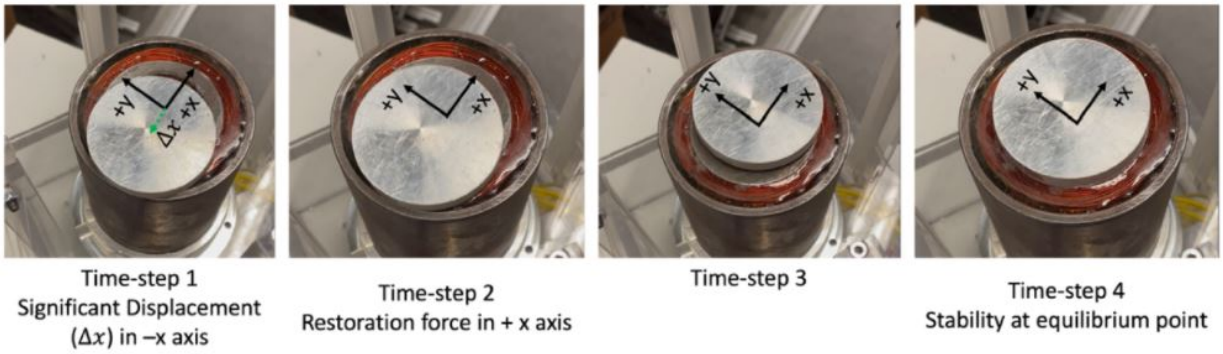

Figure 6.4: Self-restoration of disc upon application of a manual external force displacing it from its origin

levitation coil. $N \times I$ is the line integral of magnetic intensity along a closed line. Greater the magnetomotive force, greater is the average force of levitation produced by the coils.

The current coils have a magnetomotive force of **600 AmpTurns** using a **5A RMS** current input. Experimentally, as well as through ANSYS Maxwell simulations, this MMF is not sufficient for the selected disc's levitation. Hence, the objective function is to maximize the MMF while retaining the restorative ability of coils. To maximize the MMF, it is decided to alter the strength of coils. The strength of coils is shown in the following equation:

$$\frac{N_1 I_1}{N_2 I_2} = \frac{N_1}{N_2} = 1.15 \tag{6.4}$$

where, I_1 and I_2 are currents flowing through inner and outer coils respectively, and are equal in magnitude. Since the chosen BK Precision 9832B power supply has a maximum output capacity of 2kW, and the system has a high impedance even at a low frequency of 50Hz, and 300V RMS, the maximum current flowing through the two coils cannot be

further increased due to hardware limitations. Thus, finding a way to split the input power through the two channels is necessary. This will in turn create a trade-off between losing some of the restorative ability of the coils to boost its levitative ability. It needs to be done without passing a higher current that could damage the coils. This can be further understood through figure 6.5.

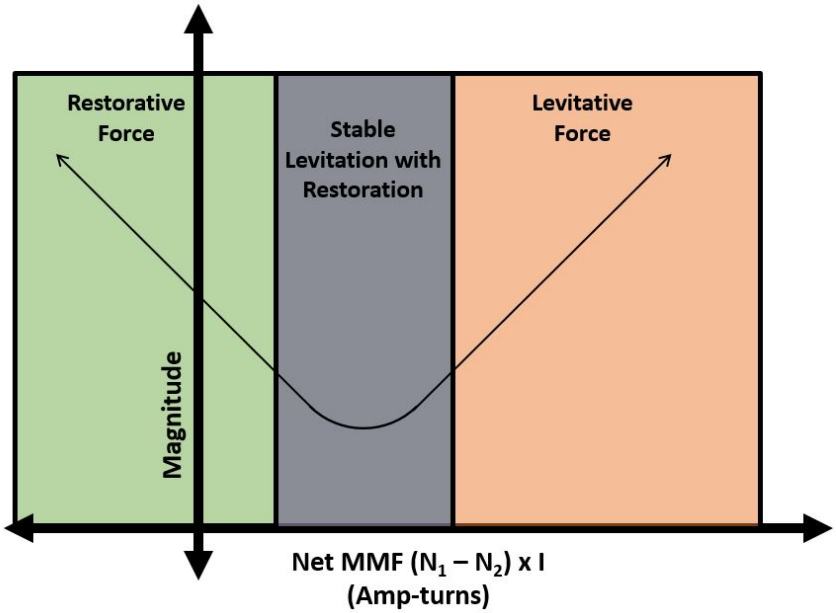

Figure 6.5: Depiction of Tradeoff between Levitation and Restoration behavior of the system. Not to scale.

In section 6.3.2, it is explained that the current through the inner coil is changed to **4.6582A RMS**, and current through the outer coil is reduced to **2.784A RMS**, and equation 6.5 shows the resulting strength of coils to be **1.9242**. This exhibits a good levitative behavior.

$$\frac{N_1 I_1}{N_2 I_2} = \frac{4.6582 \times 920}{2.784 \times 800} = 1.9242 \tag{6.5}$$

6.3.2 Variable Resistor Enclosure

From experimental analyses it is evident that the MMF of the outer coil, and thus current passing through it, needs to be reduced to facilitate the increase of levitative ability of the inner coil. This was accomplished by using a variable resistor enclosure in parallel to the outer coil. This enclosure is constructed in compliance with CSA guidelines [34], to be compatible with the AM environment. This circuit can be visualized as shown in the figure 6.6.

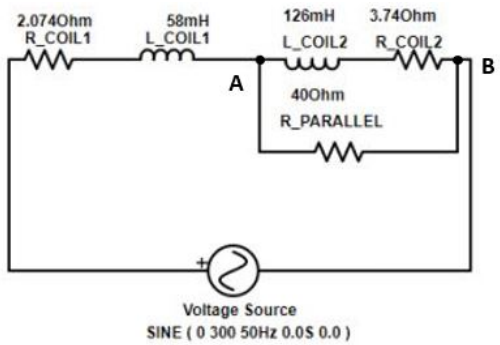

Figure 6.6: Circuit model of the coils with a 40Ω resistor in parallel to the outer coil

The current passing through the circuit splits at junction 'A' resulting in a lower current passing through the outer coil. This behavior can be further altered by using different numerical resistance values in parallel with the outer coil, at different frequencies, and an optimal value is picked for observed levitation. A parallel resistance of **40Ω**, along with

input frequency **85Hz** results in a current through inner coil equivalent to **4.6582A RMS**, and current through the outer coil as **2.784A RMS**. This is selected based on experimental and simulation results as both the domains exhibit levitation.

6.4 Successful Levitation

Based on the analytical model constructed for the circuit presented in 6.6, successful levitation of the disc is observed at 300V RMS, 85Hz. The simulation response from ANSYS Maxwell is shown in figures 6.7a and 6.7b.

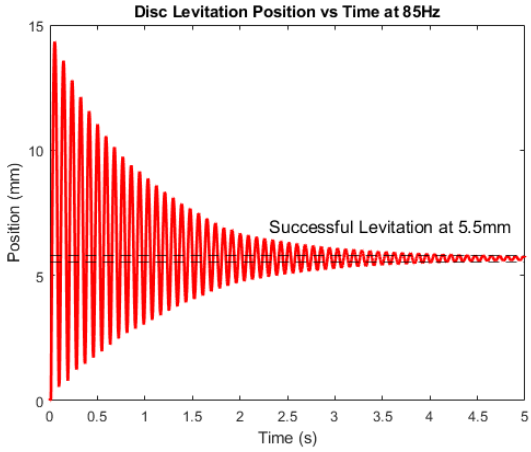

(a) Axial Position vs Time

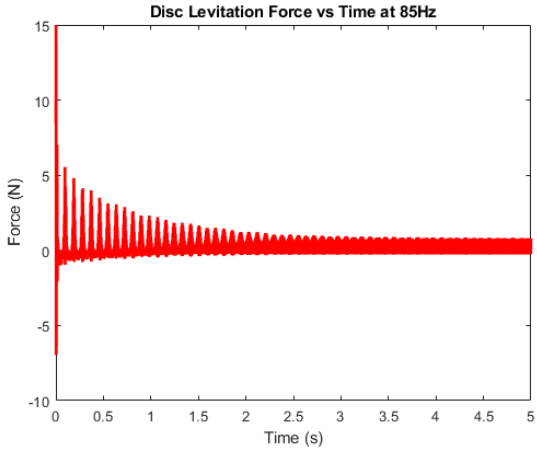

(b) Levitation Force vs Time

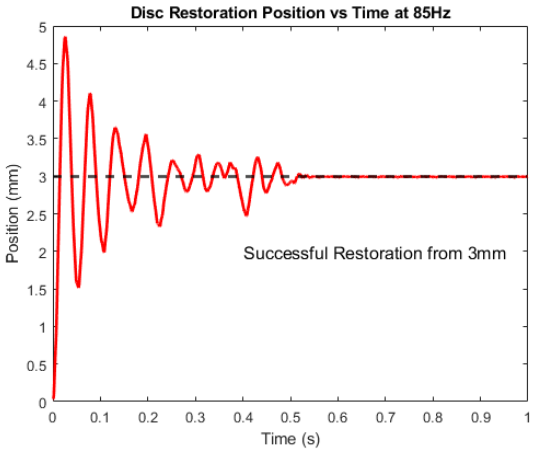

(c) Lateral Position vs Time

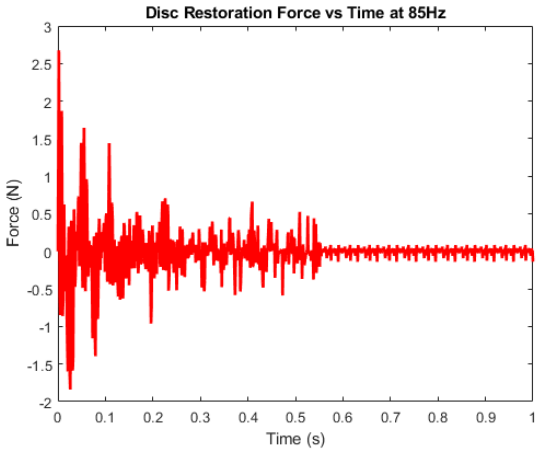

(d) Restoration Force vs Time

Figure 6.7: ANSYS Maxwell simulations at 300V RMS, 85Hz

Experimental levitation position is observed at **5mm**, as seen in figure 6.8, and ANSYS Maxwell stable levitation is noted at **5.5mm**, resulting in a net error of **9%** , which is deemed acceptable. This error exists due to the complexity of modelling this system in ANSYS Maxwell, and due to meshing errors. The disc restoration from a lateral displacement of **3mm** is also plotted using ANSYS Maxwell, and is shown in figure 6.7. Hence, the functionality of these electromagnetic coils is successfully confirmed.

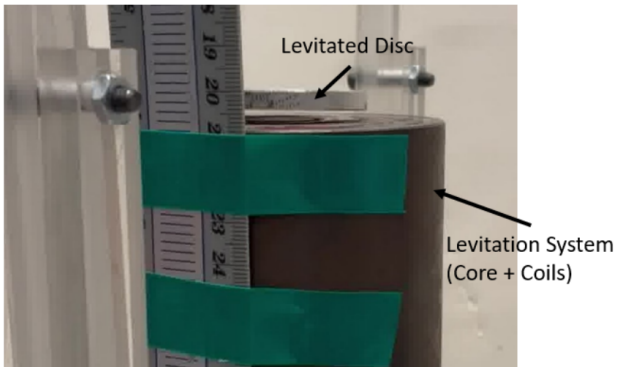

Figure 6.8: Successful experimental levitation of disc observed at 300V RMS, 85Hz

6.5 Levitation with Payload

The main purpose of conducting this research is to provide viability of the electromagnetic system function in an additive manufacturing environment. A Laser Powder Bed Fusion (LPBF) based additive manufacturing machine is chosen. The DMD IC-106 [9] is a metal based AM machine, and is deemed suitable for the application of this research. In order to replicate the levitator coil system behavior in this environment, different payloads are considered to confirm stable levitation of the fabricated substrate.

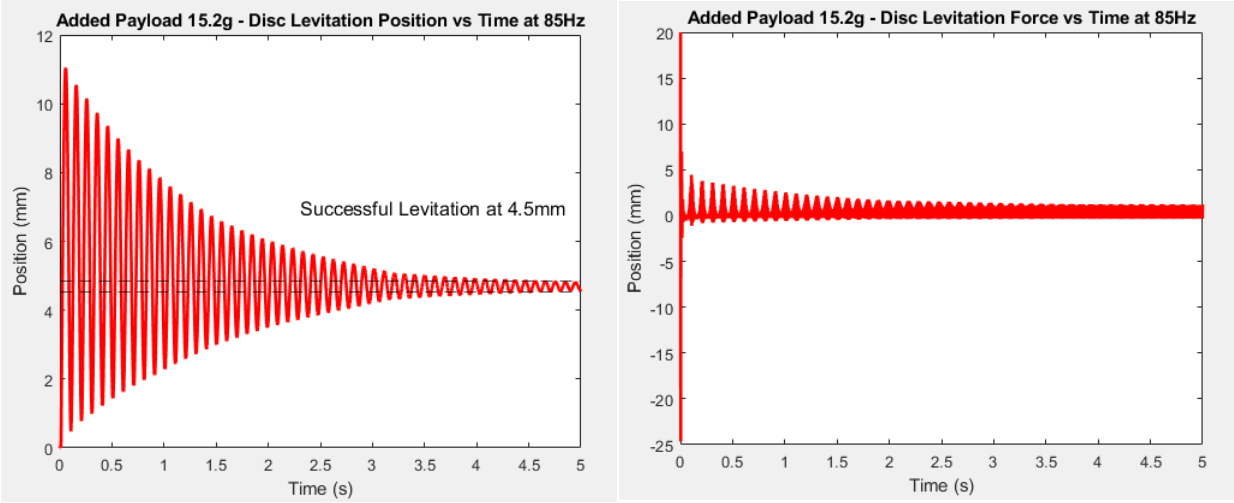

(a) Axial Position vs Time (b) Levitation Force vs Time

Figure 6.9: ANSYS Maxwell simulations with added **15.2g payload**, at 300V RMS, 85Hz

The DMD IC-106 AM machine has the capability to deposit metal powder at a rate of 5g/min. This makes it necessary to see successful disc levitation with added payloads to show compatibility with the AM environment. Experimentally, a mass of **15.2g** of a polycarbonate block is attached to the disc. A voltage of 300V RMS is applied at 85Hz, and stable levitation position is noted. This is also correlated with ANSYS Maxwell simulations, as seen in figure 6.9.

Experimental levitation position is observed at **4mm**, and ANSYS Maxwell stable levitation is noted at **4.5mm**, resulting in a net error of **11.1%** , which is deemed acceptable. This can be attributed to meshing errors in ANSYS Maxwell. The experimental levitation can be seen in figure 6.10. Therefore, the viability of using this electromagnetic coil system is proven for the AM environment.

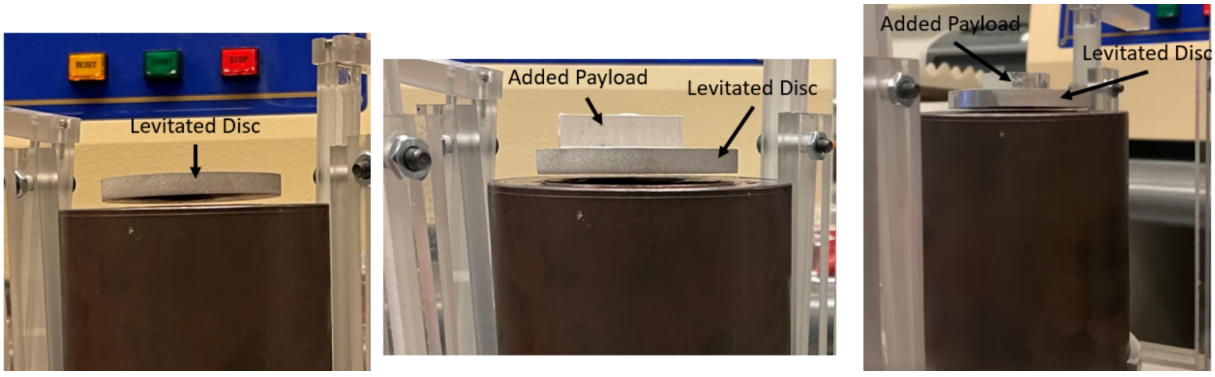

Figure 6.10: Successful experimental levitation of disc with **15.2g** added payload observed at 300V RMS, 85Hz

As ANSYS Maxwell is a reliable tool to predict the system performance with a low error in comparison to the experimental system, levitation of disc with different payloads can be simulated, as shown in figure 6.11. Different payloads of 5g, 10g, 25g, and 50g are simulated to be added to the disc mass in ANSYS Maxwell. Steady state levitation height variation is plotted against time. Simulations show successful levitation in each one of the cases mentioned. It is important to note, that the position of the disc can be controlled by changing the current or the frequency of the AC supply. As current increases, or frequency of supply decreases, the disc will move axially upward, and vice versa. This will be important to navigate the disc in the axial direction in the AM environment. This successfully fulfils a major goal of this research.

It must also be noted, that in every case of levitation observed through lab experimentation and ANSYS Maxwell simulations, the settled disc has minimal perturbations. According to ANSYS Maxwell, the disc perturbations fall within $\pm 0.2mm$, which is lesser than the

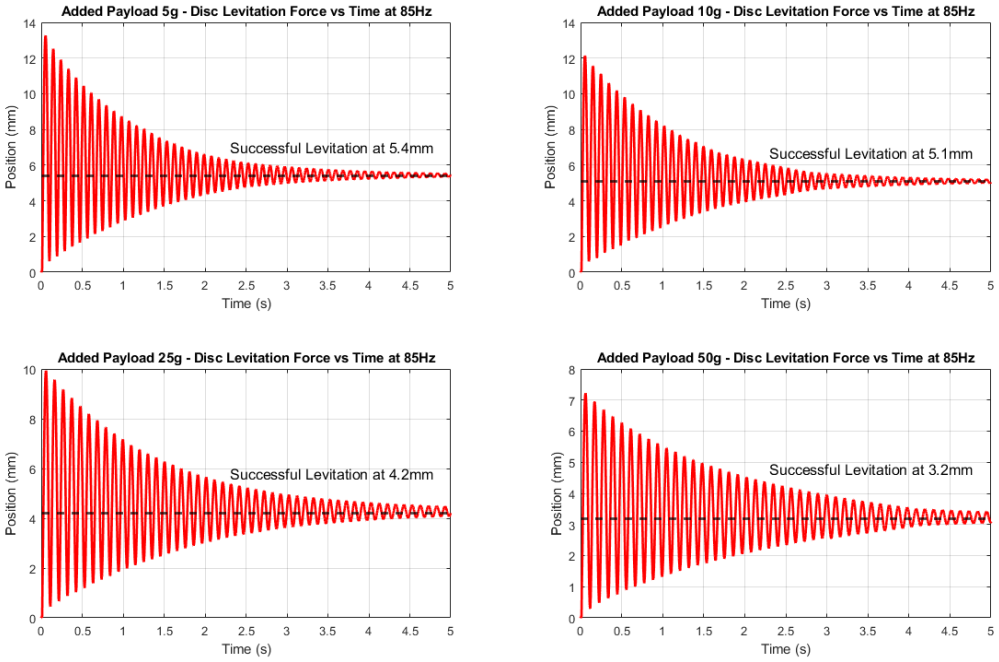

Figure 6.11: Successful simulation of levitation of disc with **5g**, **10g**, **25g**, and **50g** added payload observed at 300V RMS, 85Hz

initial target value of $\pm 0.5mm$, making the levitation acceptable.

Chapter 7

Conclusions and Future Work

This chapter mentions an overall summary of the entire research, along with discussions about some critical aspects of the electromagnetic system and its characteristics. This is followed by information on proposed ideas for future work and objectives that can be fulfilled under this project.

7.1 Summary

The purpose of this research is to design and develop a system to merge the applications of electromagnetic levitation and additive manufacturing. A multi-coil multi-core system, with two anti-parallel concentric alternating current carrying coils, is manufactured to stably levitate an Aluminum disc substrate using electrodynamic suspension (EDS). Enclosures are developed to support the high voltage application of the system, and to be compatible with the additive manufacturing environment. System is analyzed on the structural, thermal,

electrical and electromagnetic front, simulated to predict ideal behavior, and successfully implemented in experimental tests.

7.2 Discussion

The following set of conclusions can be drawn from this research:

- The integration of magnetic levitation with the additive manufacturing environment has never been accomplished before. This research accomplishes to bridge the two highly important scientific fields.
- An electromagnetic suspension technology based system can be set up using two anti-parallel concentric current carrying coils to achieve levitation for a paramagnetic object.
- Despite a lack of analytical models to design a multi-coil multi-core system it is possible to optimize its dimensions using a method of parametrization for the maximum levitation force.
- Current and frequency can be controlled to influence the height of disc levitation, hence, providing the substrate a high degree of freedom.
- Modification of strength of coils, and manipulation of the net magnetomotive force, is a feature that has minimal to no references, and has been actively worked upon to assist in levitation.

7.3 Future Work

Several aspects of this research have potential to be improved in future iterations of conceptual design. Some of them are mentioned as follows:

- The electromagnetic levitation setup presented in this research has its viability proven through ANSYS Maxwell simulation, and experimental work. The compatibility of the system has been proven to the extent of successfully levitating an added payload on top of the disc. This work can further be enhanced by incorporating this system into the additive manufacturing environment. As mentioned in earlier sections, the coils have been designed for eventual operation in the DMD IC-106 AM machine. Having proven the successful viability for electromagnetic levitation for additive manufacturing, the natural next step is to operate this system in the aforementioned machine.

- The current system is cylindrical in shape, producing time-varying magnetic fields which are axissymmetric. This can only be used to levitate an object which itself is axissymmetric, such as a cylindrical disc, as mentioned in this research. A possible future iteration of coils could introduce a change in shape to rectangular (cuboidal) for instance, to provide additional degrees of freedom, or be able to levitate non-axissymmetric objects as well.

- An important design objective of this research was to select a core material with the highest relative permeability with little regard to its counter impacting properties. Maximization of the levitation force objective function was performed which led to

an equally impactful increase in the inductive cost function. This led to lower overall current and magnetic flux density. This can be improved in future iterations by developing optimization algorithms with an objective to minimize cost function while maximizing the force experienced by the suspended disc.

- A solid core was selected because of its impact on the levitation forces experienced by the disc. This also led to core losses causing high temperatures in the system after a few minutes of operation. This problem can be avoided in the future by using laminated sheets of electric steel, as they have a substantial permeability, as well as help in minimizing and eliminating core losses.

- Future iterations of coils can be developed by increasing the net outer diameter of the system. During optimization of the system dimensions, the high inductive cost function was encountered. With an outer diameter greater than 90mm, the inductive effects of this system can be reduced. The initial constraint was developed being cognizant of the volumetric constraints of the DMD IC-106 LPBF additive manufacturing system, and future iterations can still be developed within the dimensional constraints of the machine.

- The thermal analysis of the current coils is conducted to provide a conservative upper limit to not be exceeded, so as not to damage the system. Future iterations of coils can incorporate a cooling mechanism by running an oil-based coolant through pipes surrounding the coils. These pipes being electrically non-conducting will not interfere with the magnetic fields of the system, and will provide a steady way of extracting heat from the coils for an AM operation that can potentially be extended from 20

minutes to much more.

- The selected power supply consists of an in-built controller which was an unused feature. Future iterations of coils can be developed with the incorporation of a closed loop feedback controller to create stability of disc levitation, as seen in figure 7.1. Hall-effect sensors, inductance sensors, position sensors as well as laser sensors have been considered for the same. The final decision will be based on the resolution of the sensor and its compatibility with the additive manufacturing environment.

- Another possible use case for sensor integration in future iterations would involve a greater focusing on requirements for additive manufacturing. Since metal deposition in AM is a dynamic process, the forces acting on the levitated substrate would also create disturbances, which, for the purpose of this research have been fixed at a maximum tolerance of $\pm 0.5mm$. For additive manufacturing practices that require a greater degree of manufacturing precision, these disturbances could further be controlled using a closed loop feedback from a sensor.

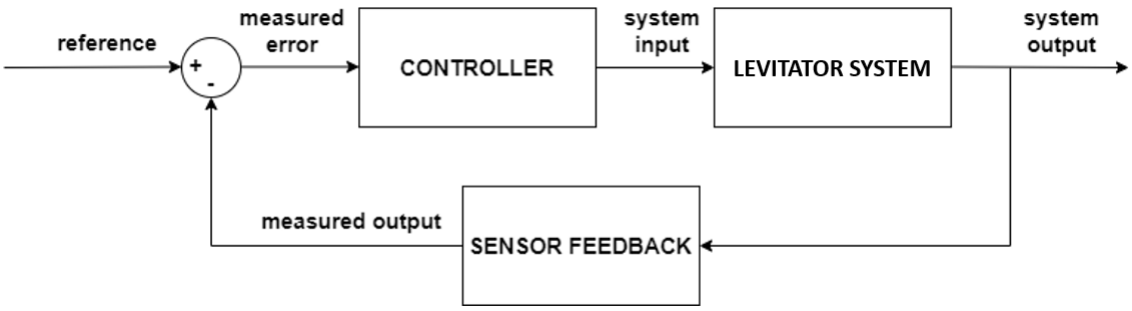

Figure 7.1: Possible control system using sensor feedback for future iterations of coils

References

[1] M. D. Simon and A. K. Geim, "Diamagnetic levitation: Flying frogs and floating magnets (invited)," *Journal of Applied Physics*, vol. 87, no. 9, pp. 6200–6204, 2000.

[2] N. Ida and J. P. Bastos, *Electromagnetics and calculation of fields*. New York, NY: Springer Science & Business Media, 2013.

[3] S. E. Boslaugh, "Maglev," *Encyclopedia Brittanica*, 2020.

[4] J. Powell, "High-speed transport by magnetically suspended trains," *ASME paper*, vol. 66, p. 1, 1966.

[5] E. Davoodi, H. Montazerian, A. S. Mirhakimi, M. Zhianmanesh, O. Ibhadode, S. I. Shahabad, R. Esmaeilizadeh, E. Sarikhani, S. Toorandaz, S. A. Sarabi, *et al.*, "Additively manufactured metallic biomaterials," *Bioactive Materials*, 2021.

[6] A. W. Gebisa and H. G. Lemu, "Additive manufacturing for the manufacture of gas turbine engine components: Literature review and future perspectives," in *Turbo Expo: Power for Land, Sea, and Air*, American Society of Mechanical Engineers, vol. 51128, 2018, V006T24A021.

[7] F. Bos, R. Wolfs, Z. Ahmed, and T. Salet, "Additive manufacturing of concrete in construction: Potentials and challenges of 3d concrete printing," *Virtual and physical prototyping*, vol. 11, no. 3, pp. 209–225, 2016.

[8] W. A. Harkness and J. H. Goldschmid, "Free-form spatial 3-d printing using part levitation," 20 160 031 156, Feb. 2016.

[9] DM3D, *Direct metal deposition technology*, `https://dm3dtech.com/technology`.

[10] D. W. Ball, "Maxwell's equations, part vii," *Spectroscopy*, vol. 27, no. 6, pp. 20–27, 2012.

[11] M. T. Thompson, "Eddy current magnetic levitation. models and experiments," *IEEE potentials*, vol. 19, no. 1, pp. 40–44, 2000.

[12] D. C. Giancoli, I. A. Miller, O. P. Puri, P. J. Zober, and G. P. Zober, "Physics: Principles with applications," 1998.

[13] D. J. Griffiths and D. F. Schroeter, *Introduction to quantum mechanics*. Cambridge University Press, 2018.

[14] J. W., "Earnshaw's theorem and the stability of matter," *European Journal of Physics*, vol. 1, no. 2, pp. 85–88, 1980.

[15] E. Cazacu and A. Moraru, "Escaping from earnshaw's theorem," *REVUE ROUMAINE DES SCIENCES TECHNIQUES SERIE ELECTROTECHNIQUE ET ENERGETIQUE*, vol. 51, no. 3, p. 275, 2006.

[16] J. Witteveen, R. van Gastel, A. van Houselt, and H. Zandvliet, "3d modeling of electromagnetic levitation coils," *Current Applied Physics*, vol. 32, pp. 45–49, 2021.

[17] F. Ghayoor and A. Swanson, "Modelling and analysis of electrodynamic suspension of an aluminium disc as a complex engineering problem," *International Journal of Electrical Engineering Education*, vol. 55, no. 2, pp. 91–108, 2018.

[18] E. Laithwaite, "Electromagnetic levitation," in *Proceedings of the Institution of Electrical Engineers*, IET, vol. 112, 1965, pp. 2361–2375.

[19] (Mar. 13, 2022). "What is the skin effect? — reactance and impedance – inductive — electronics textbook," [Online]. Available: `https://www.allaboutcircuits.com/textbook/alternating-current/chpt-3/more-on-the-skin-effect/` (visited on 03/15/2022).

[20] P. Kazemzadeh Heris and M. B. Khamesee, "Design and fabrication of a magnetic actuator for torque and force control estimated by the ann/sa algorithm," *Micromachines*, vol. 13, no. 2, p. 327, 2022.

[21] Z. L. Royer, C. Tackes, R. LeSar, and R. E. Napolitano, "Coil optimization for electromagnetic levitation using a genetic like algorithm," *Journal of Applied Physics*, vol. 113, no. 21, p. 214 901, 2013.

[22] (Mar. 8, 2022). "Proper coil drive: Critical to good relay/contactor performance — te connectivity," [Online]. Available: `https://www.te.com/usa-en/products/relays-contactors-switches/relays/intersection/coil-drive-relay-contactor-performance.html?tab=pgp-story` (visited on 03/08/2022).

[23] R. Wills, "I. effects of temperature on the magnetic properties of iron and alloys of iron," *The London, Edinburgh, and Dublin Philosophical Magazine and Journal of Science*, vol. 50, no. 302, pp. 1–37, 1900.

[24] E. Zaretsky and G. Kanel, "Response of copper to shock-wave loading at temperatures up to the melting point," *Journal of Applied Physics*, vol. 114, no. 8, p. 083 511, 2013.

[25] T. J. Ahrens, K. G. Holland, and G. Q. Chen, "Shock temperatures and the melting point of iron," in *AIP Conference Proceedings*, American Institute of Physics, vol. 429, 1998, pp. 133–136.

[26] (May 14, 2020), [Online]. Available: `https://www.crosslinktech.com/data_sheets/ul_recognized/CLR1331_CLH5515.pdf` (visited on 03/08/2022).

[27] (Jul. 25, 2016). "Electrical power in ac circuits and reactive power," [Online]. Available: `https://www.electronics-tutorials.ws/accircuits/power-in-ac-circuits.html` (visited on 03/09/2022).

[28] D. Lin, P. Zhou, W. Fu, Z. Badics, and Z. Cendes, "A dynamic core loss model for soft ferromagnetic and power ferrite materials in transient finite element analysis," *IEEE Transactions on magnetics*, vol. 40, no. 2, pp. 1318–1321, 2004.

[29] (Aug. 3, 2016), [Online]. Available: `http://ridleyengineering.com/images/phocadownload/7%5C%20modeling%5C%20ferrite%5C%20core%5C%20losses.pdf` (visited on 03/09/2022).

[30] B. Grabowski, L. Ismer, T. Hickel, and J. Neugebauer, "Ab initio up to the melting point: Anharmonicity and vacancies in aluminum," *Physical Review B*, vol. 79, no. 13, p. 134 106, 2009.

[31] F. W. Grover, *Inductance calculations: working formulas and tables*. Courier Corporation, 2004.

[32] (Mar. 2, 2022). "Discontinued model 2567, 70 mhz, 100 mhz, 200 mhz, and 300 mhz 2 gsa/s dso and mso - bk precision," [Online]. Available: https://www.bkprecision.com/products/oscilloscopes/2567-200-mhz-2-gsa-s-4-channel-dso.html (visited on 03/02/2022).

[33] (Feb. 28, 2022). "Magnetomotive force - an overview — sciencedirect topics," [Online]. Available: https://www.sciencedirect.com/topics/engineering/magnetomotive-force (visited on 02/28/2022).

[34] *Class 1 and class 2 circuits*, 2018.

Appendices

Appendix A

Coil and Core Schematics

The following pages contain the engineering drawings for the coils and core in the system.

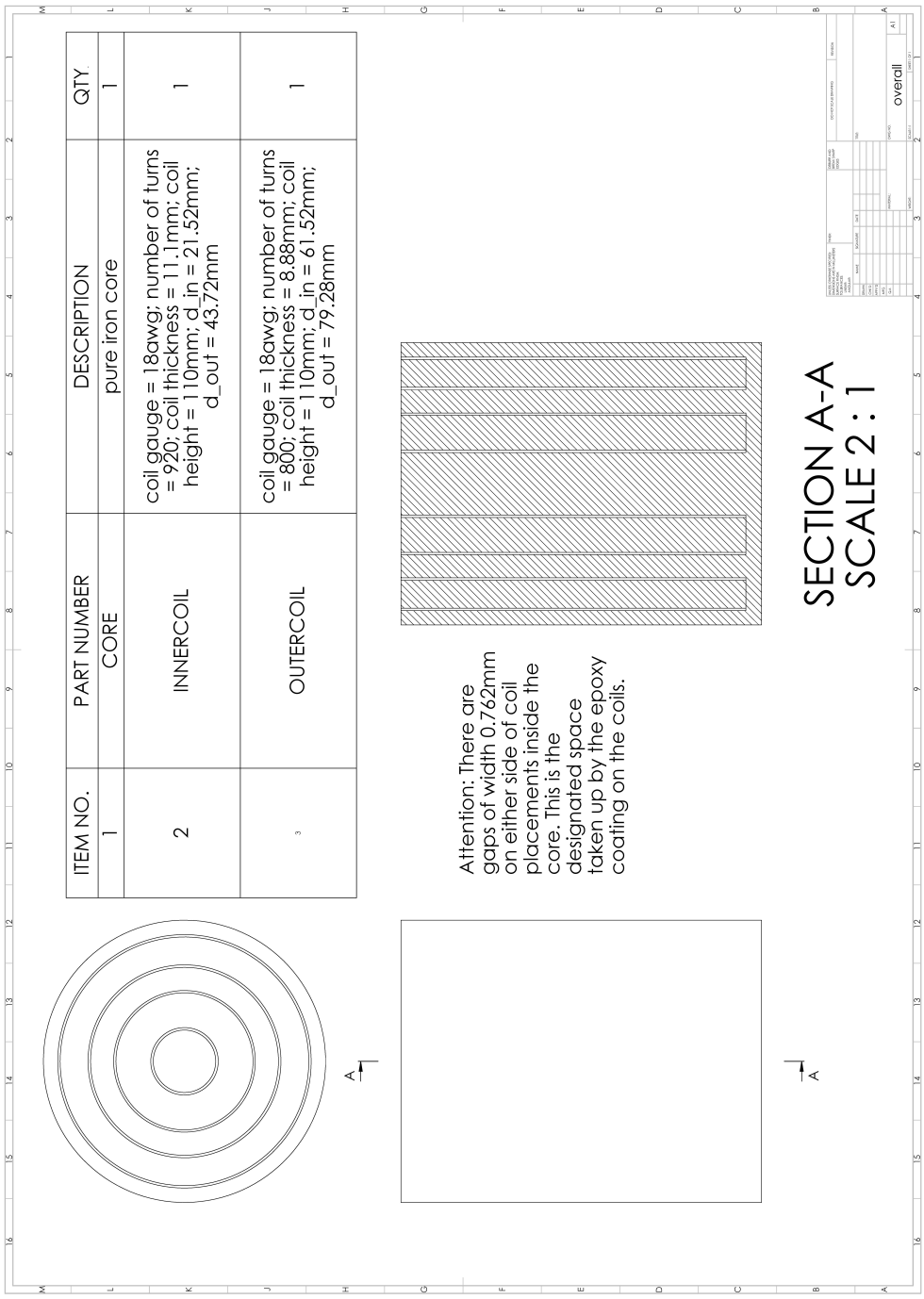
ITEM NO.
PART NUMBER
DESCRIPTION
QTY
1
CORE
pure iron core
1
2
INNERCOIL
coil gauge = 18awg; number of turns = 920; coil thickness = 11.1mm; coil height = 110mm; d_in = 21.52mm; d_out = 43.72mm
1
3
OUTERCOIL
coil gauge = 18awg; number of turns = 800; coil thickness = 8.88mm; coil height = 110mm; d_in = 61.52mm; d_out = 79.28mm
1
A
A
Attention: There are gaps of width 0.762mm on either side of coil placements inside the core. This is the designated space taken up by the epoxy coating on the coils.
SECTION A-A
SCALE 2 : 1
overall

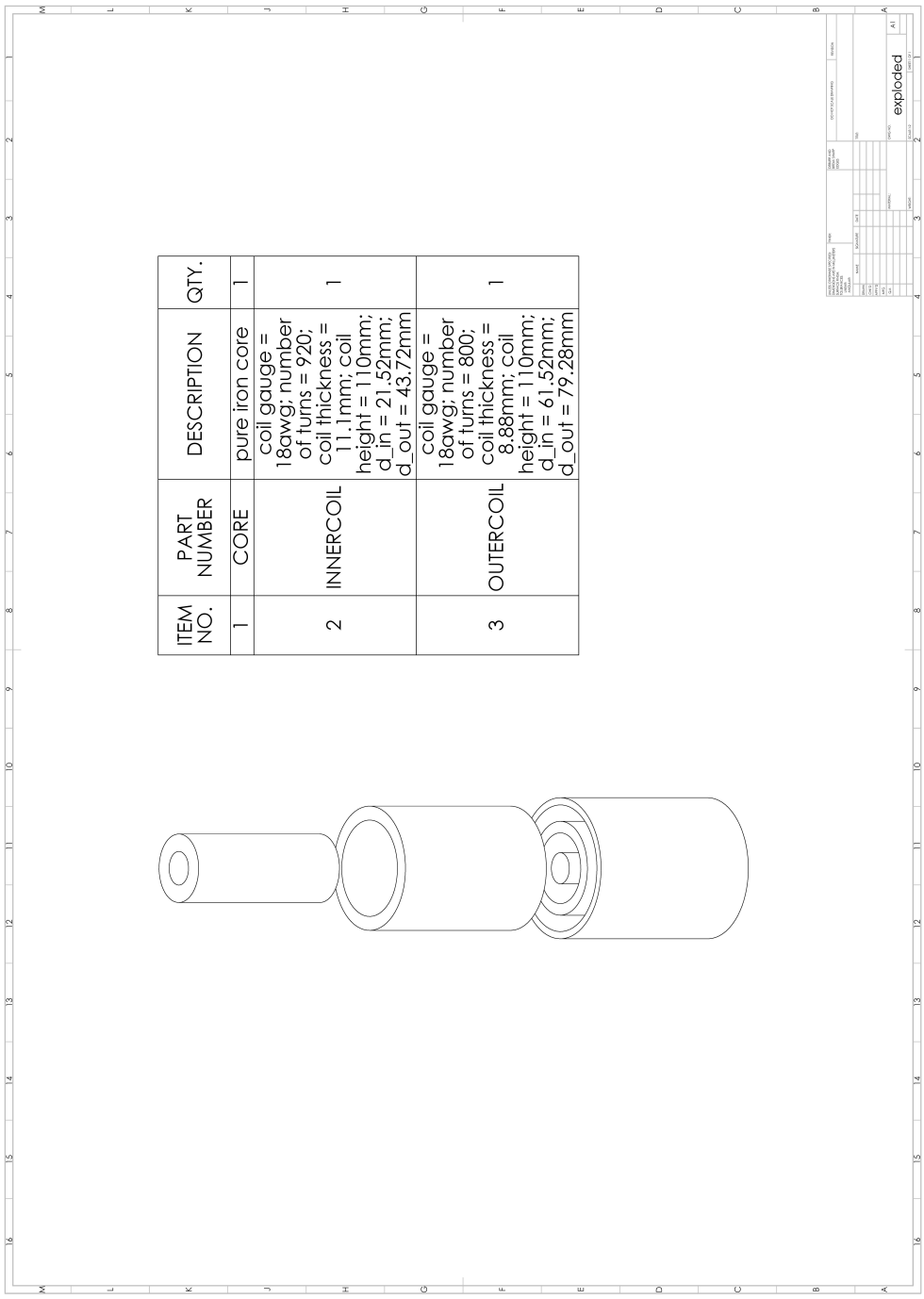

ITEM NO.	PART NUMBER	DESCRIPTION	QTY.
1	CORE	pure iron core	1
2	INNERCOIL	coil gauge = 18awg; number of turns = 920; coil thickness = 11.1mm; coil height = 110mm; d_in = 21.52mm; d_out = 43.72mm	1
3	OUTERCOIL	coil gauge = 18awg; number of turns = 800; coil thickness = 8.88mm; coil height = 110mm; d_in = 61.52mm; d_out = 79.28mm	1

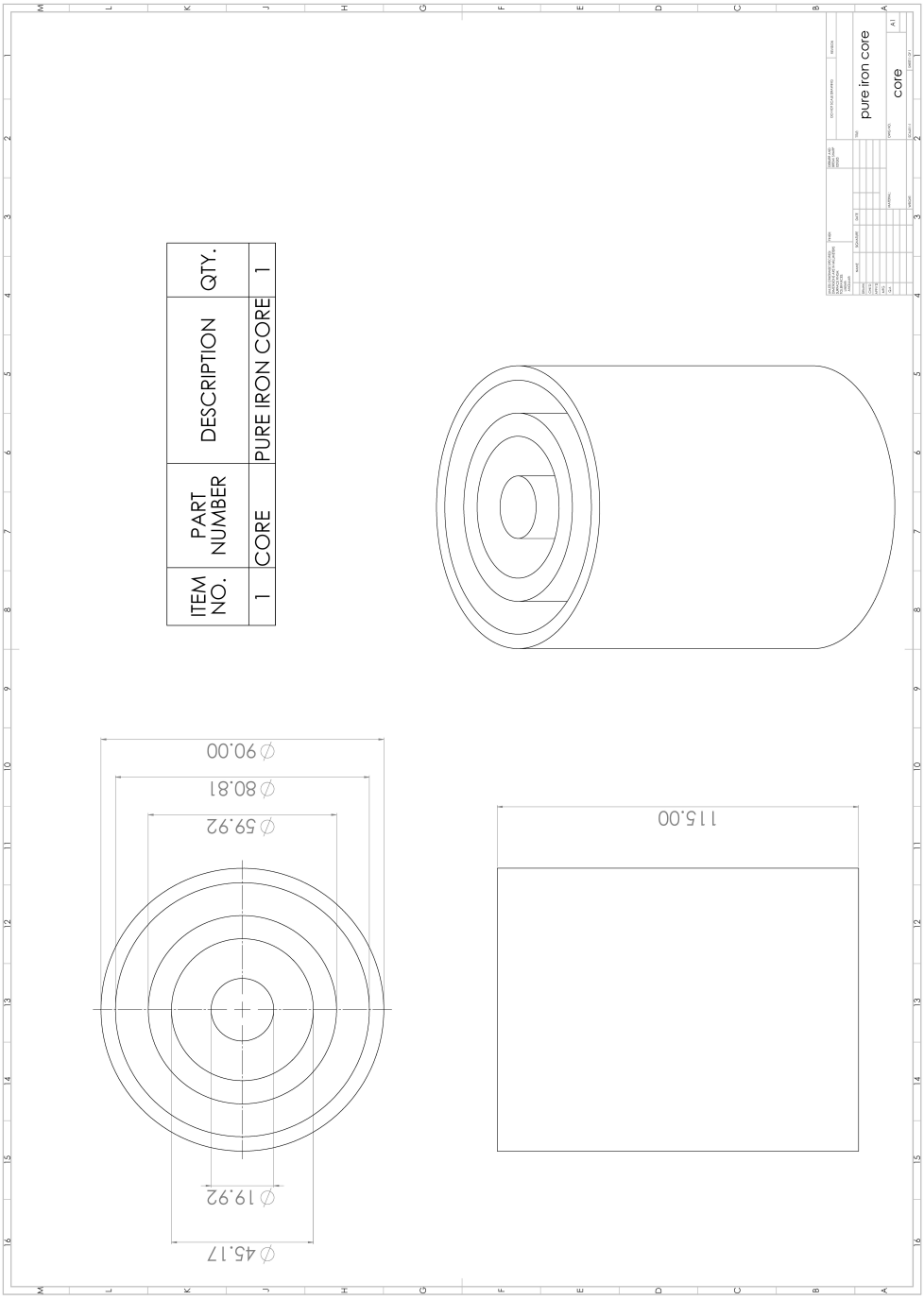
pure iron core
core
ITEM NO.
PART NUMBER
DESCRIPTION
QTY.
1
CORE
PURE IRON CORE
1
∅90.00
∅80.81
∅59.92
∅19.92
∅45.17
115.00

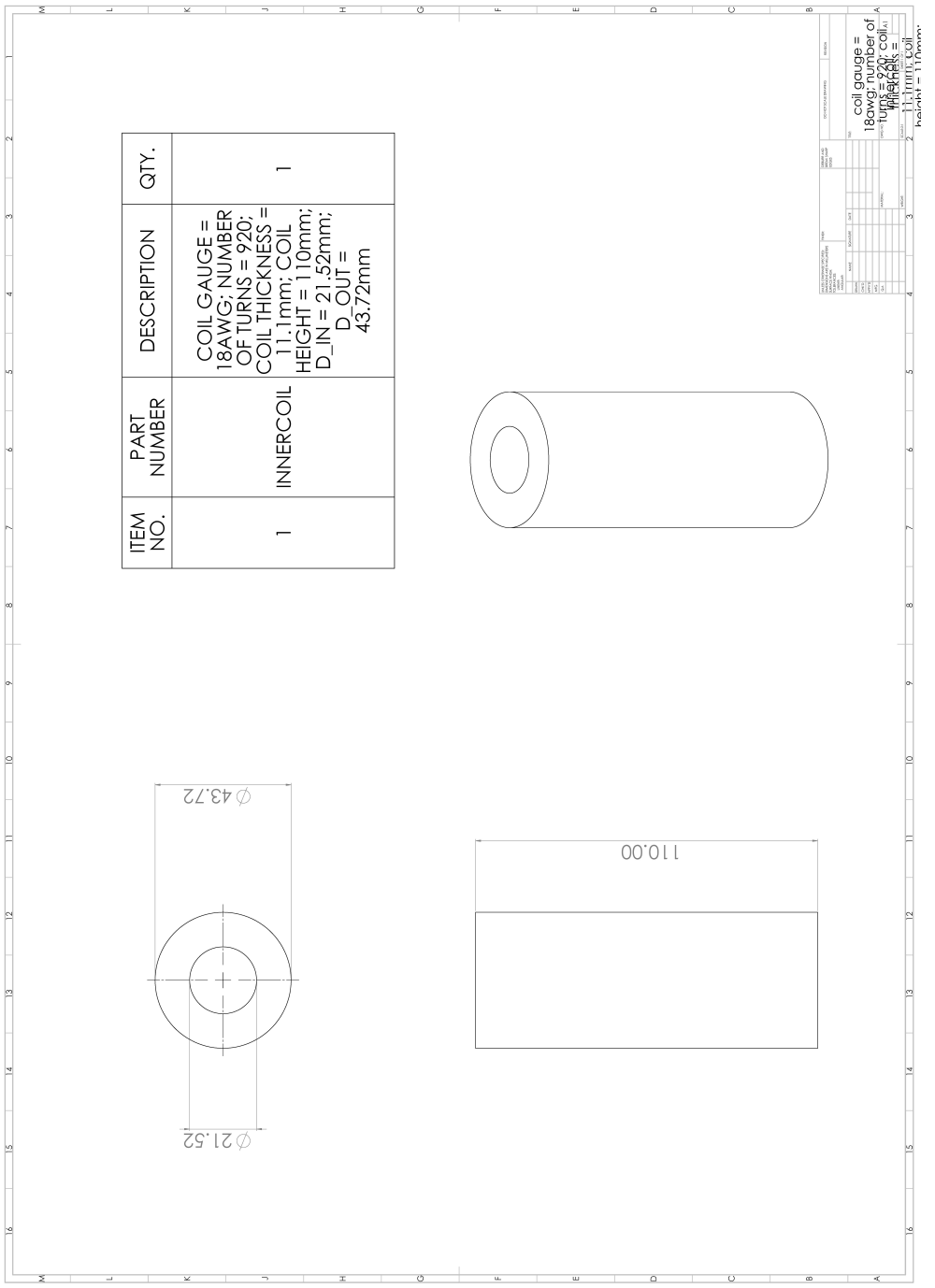
ITEM NO.
PART NUMBER
DESCRIPTION
QTY.
1
INNERCOIL
COIL GAUGE = 18AWG; NUMBER OF TURNS = 920; COIL THICKNESS = 11.1mm; COIL HEIGHT = 110mm; D_IN = 21.52mm; D_OUT = 43.72mm
1
coil gauge = 18awg; number of turns = 920; coil thickness = 11.1mm; coil height = 110mm;
110.00
∅43.72
∅21.52

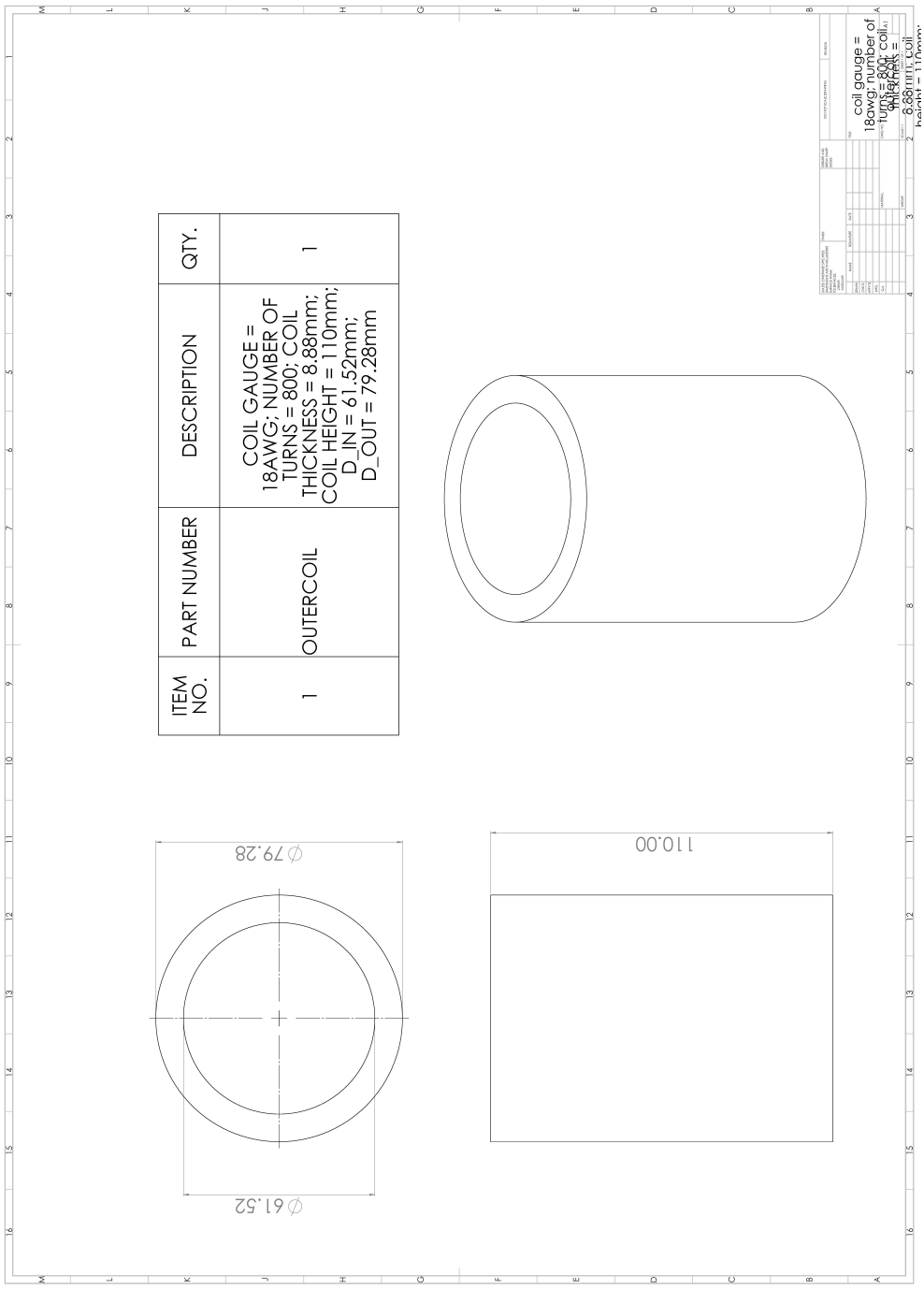
ITEM NO.
PART NUMBER
DESCRIPTION
QTY.
1
OUTERCOIL
COIL GAUGE = 18AWG; NUMBER OF TURNS = 800; COIL THICKNESS = 8.88mm; COIL HEIGHT = 110mm; D_IN = 61.52mm; D_OUT = 79.28mm
1
110.00
∅79.28
∅61.52